Han, Y., Noah, M., Lüders, V., Körmös, S., Schubert, F., Pötz, S., Horsfield, B., Mangelsdorf, K. (2022): Fractionation of hydrocarbons and NSO-compounds during primary oil migration revealed by high resolution mass spectrometry: Insights from oil trapped in fluid inclusions. - International Journal of Coal Geology, 254, 103974.

https://doi.org/10.1016/j.coal.2022.103974

Fractionation of hydrocarbons and NSO-compounds during primary oil migration revealed by high resolution mass spectrometry: insights from oil trapped in fluid inclusions

Yufu Han[a], Mareike Noah[a], Volker Lüders[a], Sándor Körmös[b], Félix Schubert[b], Stefanie Poetz[a], Brian Horsfield[a,c] , Kai Mangelsdorf[a]

[a]Helmholtz Centre Potsdam GFZ – German Research Centre for Geosciences, Section 3.2 Organic Geochemistry, Telegrafenberg, 14473 Potsdam, Germany

[b]University of Szeged, Department of Mineralogy, Geochemistry and Petrology, H-6722, Szeged, Egyetem utca 2, Hungary

[c]GEOS4 GmbH, D-14552 Michendorf, Germany

* Corresponding author: Email address: yhan@gfz-potsdam.de,

Tel: +49 331-288-28688

Abstract

The composition of oil trapped in fluid inclusions (FI), occurring in mineral cements, can provide valuable insights into oil migration. Here, FI oils in a calcite vein (representing expelled fluids) and source rock (SR) extracts (representing retained bitumen) from the Hosszúhetény Calcareous Marl Formation (HCMF) in the Mecsek Mountains area of Hungary were investigated to assess how organic compounds are fractionated during primary migration. Biomarkers analyzed by gas chromatography-mass spectrometry and gas chromatography-stable carbon isotope ratio mass spectrometry were used to demonstrate that the FI oils had been expelled from the HCMF marl (calculated vitrinite reflectance of ~ 0.74% Rc). Fourier

transform-ion cyclotron resonance-mass spectrometry then provided insights into polar compound geochemistry, showing that O_1, N_1, N_1O_1 and S_1O_1 compound classes are preferentially retained in the source rock bitumen, while less polar compounds like aromatic hydrocarbons (HCs) and S_1 compounds are assumed to be preferentially expelled. Independent of the compound class, compounds with higher double bond equivalents (DBEs) are enriched in the retained source rock bitumen. Thus, besides the molecular polarity determined by the functional groups, the molecular size and the degree of aromaticity appear to be the most important factors affecting the migration and retention behavior of the petroleum HCs and NSO-compounds in the HCMF. Moreover, the enrichment of high DBE compounds with shorter alkyl chains in the SR extracts infers that shielding effects could have played a major role for compound retention and expulsion during primary oil migration.

Key words: FI oil, NSO-compounds, oil primary migration, FT-ICR-MS, Hosszúhetény Calcareous Marl Formation, petroleum fractionation

1 Introduction

During primary oil migration, petroleum is expelled from the source rock into the surrounding or adjacent carrier lithology. During this process the expelled fluids become enriched in saturated hydrocarbons, while the retained bitumen is enriched in asphaltenes and resins (Tissot and Welte, 1984). The expulsion sequence saturated hydrocarbons > aromatic hydrocarbons > polar compounds has been confirmed using

45 experiments and modelling in many studies (Tissot and Welte, 1984; Leythaeuser et
46 al., 1988a; Sandvik et al., 1992; Kelemen et al., 2006; Han et al., 2015). The
47 preferential expulsion of saturated hydrocarbons and aromatic compounds has been
48 widely examined using gas chromatography either coupled to a flame ionization
49 detector (GC-FID) or a mass spectrometer (GC-MS) (Mackenzie et al., 1983;
50 Leythaeuser et al., 1988b, 1998c; Han et al., 2015). For example, Mackenzie et al.
51 (1983) showed that a preferential expulsion of lower carbon number *n*-alkanes occurs
52 during migration. Han et al. (2015) elucidated the preferential retention of polar
53 compounds, aromatic hydrocarbons and saturated hydrocarbons in this order within
54 the Barnett shale. In addition to natural reservoir and source rock units (Tissot and
55 Welte, 1984; Leythaeuser et al., 1988a; Han et al., 2015; Mahlstedt et al., 2016) also
56 expulsion simulation experiments (Mohnhoff et al., 2016; Stockhausen et al., 2019,
57 2020, 2021) have been applied to examine oil migration and expulsion processes.
58 Furthermore, compositional fractionation processes during migration can be assessed
59 by nitrogen, sulfur and oxygen (NSO)-containing compounds, e.g., methylcarbazoles
60 and xanthones (Larter and Aplin, 1995; Li et al., 1995; Larter et al., 1996; Taylor et al.,
61 1997; Clegg et al., 1998; Oldenburg et al., 2002; Bennett et al., 2004), because, due to
62 their polarity, these compounds are most strongly influenced by physical and chemical
63 interaction processes with the pore fluids and the surrounding mineral and organic
64 matrix. The relative enrichment of nitrogen-shielded and nitrogen-exposed
65 benzocarbazole isomers were used to elucidate the fractionation during migration (Li
66 et al., 1995), although a strong link to maturity occurs in the case of vertically charged

petroleum systems (Clegg et al., 1998; Horsfield et al., 1998). Phenols and its alkylated homologues can alter wetting properties of mineral surface, subsequently allowing the adsorption of larger hydrophobic molecules (Larter and Aplin, 1995; Taylor et al., 1997; Bennett et al., 2004). While these low molecular weight NSO-containing compounds have intensively been investigated to study oil migration processes (Leythaeuser et al., 1988c; Yamamoto et al., 1991; Li et al., 1995; Peters et al., 2018), studies on high molecular weight NSO-compounds are rare.

Fourier transform-ion cyclotron resonance-mass spectrometry (FT-ICR-MS) has broadened the analytical window for NSO-compounds and aromatic hydrocarbons (HCs) (Marshall and Rodgers, 2008). The ultra-high mass resolution allows the elemental composition of thousands of previously inaccessible organic compounds to be determined and thus allows new insights into compositional fractionation processes to be gained. Numerous studies have been conducted to address the aromatic HC and NSO-compound fractionation during oil migration by investigating the free petroleum phase using Electrospray Ionization (ESI) and Atmospheric Pressure Photoionization (APPI) FT-ICR-MS (Mahlstedt et al., 2016; Han et al., 2018a, 2018b, 2021; Ziegs et al., 2018; Poetz et al., 2020; Yue et al., 2021). The migration related fractionation is controlled by the elemental classes with their different functional groups and polarities (Han et al., 2018a, 2018b, 2021; Ziegs et al., 2018; Poetz et al., 2020; Yue et al., 2021). Han et al. (2018a, 2018b) pointed out that the N_y compounds were selectively retained in the Mississippian Barnett Shale, while the N_yO_x compounds were preferentially expelled. The opposite case has been reported in the Eagle Ford

89 petroleum system, here pyrrolic nitrogen compounds are more enriched in crude oil,
90 while high contents of N_yO_x and S_zO_x compounds remained in the source rock (Poetz
91 et al., 2020). Retention of NSO-compounds in source rock also depends on their
92 molecular size and aromaticity (Mahlstedt et al., 2016; Poetz et al., 2020; Yue et al.,
93 2021). Mahlstedt et al. (2016) revealed that the aromaticity and molecular size of
94 NSO-compounds increased much more pronouncedly with increasing maturity for
95 retained than for expelled oil. The lithofacies of source rock was considered to play a
96 significant role on oil expulsion as well. For instance, Yue et al. (2021) reported that
97 nitrogen-containing compounds are preferentially retained by biogenic quartz of the
98 Barnett Shale, while the more polar acidic oxygen-containing compounds are
99 preferably retained by clay-rich Posidonia Shale, exhibiting various retention
100 capacities of NSO-compounds with respect to the mineralogical compositions.

101 Oil-bearing fluid inclusions (FIs) hosted in mineral cements contain aliquots of
102 oil that were trapped either within cavities during crystal growth, in which case they
103 are termed primary FIs, or during subsequent recrystallization, in which case they are
104 termed secondary FIs (Burruss, 1981). The great advantage of investigating FI oils is
105 that the oil is physically isolated, and therefore its composition is not affected by later
106 secondary geological transformation processes (Volk and George, 2019). The
107 geochemical information they contain has been used to compare present oil properties
108 with those of paleo-oils (early oil charges) and to examine the impact of migration
109 and alteration processes on oil composition (Horsfield and McLimans, 1984; Bodnar,
110 1990; Jochum et al., 1995; Volk et al., 2002; George et al., 2007; Cobbold et al., 2013;

111 Volk and George, 2019). Recently, a procedural and analytical protocol for analyzing
112 aromatic HCs and NSO-compounds in FI oils using FT-ICR-MS has been reported
113 (Noah et al., 2018; Han et al., 2020, 2022). The ultra-high mass resolution allows the
114 elemental composition of thousands of newly accessible organic compounds to be
115 identified.

116 In the study reported here, we have compared the solvent extracts from two marl
117 source rock (SR) samples from the Hosszúhetény Calcareous Marl Formation (HCMF)
118 (Hungary) with six FI oil samples hosted in a calcite vein cutting the HCMF in order
119 to unravel the compositional fractionation of aromatic HCs and NSO-compounds
120 during oil primary migration. In a first step, biomarker and stable carbon isotope
121 analyses were conducted using GC-MS and gas chromatography-isotope ratio mass
122 spectrometry (GC-IRMS) to establish compositional relationships between SR
123 extracts (retained bitumen) and FI oils (expelled oil). In addition to these conventional
124 methods, FT-ICR-MS in APPI positive (+) mode was then applied to reveal effects of
125 migration-induced fractionation on the petroleum HCs and NSO-compounds.

126 # 2 Geological setting and sample set

127 ## 2.1 Geological setting

128 The Pannonian Basin is surrounded by the Dinarides, Alps and Carpathians (Fig.
129 1a). The Mecsek Mountains are located in the southwestern part of the Pannonian
130 Basin. The mountain range forms part of the Tisza Mega-unit (Csontos, 1995; Csontos
131 et al., 2002). This area became part of the European continent at the end of the
132 Variscan orogeny, and rifted off the European shelf at the end of the Jurassic (Haas et

al., 1999; Csontos et al., 2002). The complex movement of crustal plates resulted in amalgamation and the Tisza Mega-unit reached its current position during the Palaeogene and Neogene (Csontos et al., 2002). An extensional half-graben formed during the Rhaetian to Hettangian time, and coal-bearing fluvial-deltaic swamp sediments of the Mecsek Coal Formation were deposited (Haas, 2012). In the early Sinemurian, the subsidence of the Mecsek Basin resulted in the deposition of shallow marine sandstones and marls of the Zobákpuszta Sandstone Formation and Vasas Marl Formation, respectively (Raucsik, 2012a, 2012b). Due to a rise in eustatic see level a bioturbated, hemipelagic series of mixed carbonate and siliciclastic sediments were deposited, comprising the HCMF (Raucsik, 2012c). The Upper Pliensbachian and Lower Toarcian succession are characterized by monotonous bioturbated, spotted marl with turbiditic sandstone intercalations (Mecseknádasd Sandstone Formation) and limestone beds (Kecskehát Limestone Formation), representing depositional conditions controlled by tectonism, sea level fluctuation and climate change (Raucsik and Varga, 2008). The lower Toarcian strata also contain organic-rich and laminated sediments of the Rékavölgy Siltstone Formation (Varga et al., 2007; Raucsik, 2012d). Spotted marl deposition succeeded black shale deposition in the remaining Toarcian (Komló Calcarous Marl Formation) (Raucsik, 2012e) (Fig. 1b).

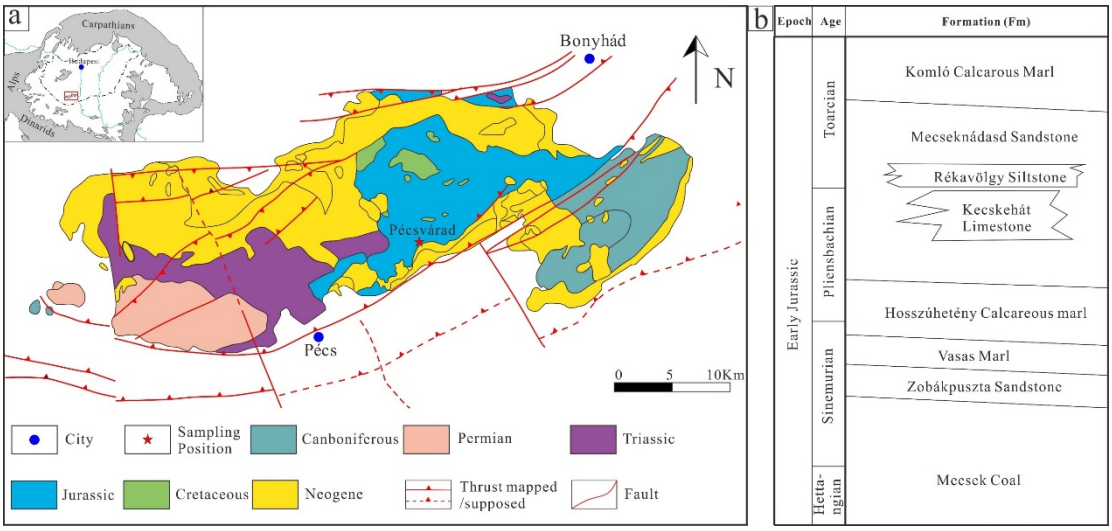

Fig. 1. a) Geological map of Mecsek Mountains in Hungary and sampling outcrop position (revised from Csontos et al. (2002) and Raucsik and Varga (2008)); b) Chronostratigraphic chart of Early Jurassic formations of Mecsek Mountain in Hungary (revised from Főzy (2012)).

The focus of the study is the Lower Jurassic Hosszúhetény Calcareous Marl Formation. Calcite-filled fractures up to 40 cm thick crosscut the thick-bedded HCMF, where abundant oil FIs have been discovered (Lukoczki et al., 2012). Although there are several potential source rocks in the Mecsek Mountains, such as the Mecsek Coal Formation, Vasas Marl Formation, Hosszúhetény Calcareous Marl Formation, and the Rékavölgy Siltstone Formation (Fig. 1b), it is the HCMF marl which is the most likely SR for the FI oils, because the calcite vein cuts through this formation and is sub-perpendicular to the HCMF marl (Fig. 2). The measured vitrinite reflectance values (Ro = 0.69%–0.73%) suggest that the sediments and incorporated organic matter are within the oil window (Lukoczki et al., 2012).

2.2 Sample set

Two source rocks (named as SR-1 and SR-2) and six pure milky-gray FI-bearing calcites (named as FI-1 to FI-6) from a vein within the HCMF were collected from an

abandoned quarry close to the town of Pécsvárad in the Mecsek Mountains, Hungary (Fig. 2). The two type II kerogen source rocks SR-1 and SR-2 (Raucsik, 2012c) are dark-grey calcareous marls with total organic carbon (TOC) contents of 0.31% and 0.63%, respectively. The Rock-Eval data for SR-1 and SR-2 indicate hydrogen index (HI = S2/TOC × 100) data of 62 and 54 mg HC/g TOC and Tmax values of 456°C and 455°C, respectively. Massive calcite fills the HCMF fractures with tens of meters in length and several to tens of centimeters in width (Fig. 2a). Calcite vein material could easily be obtained and split into small pieces (Fig. 2b).

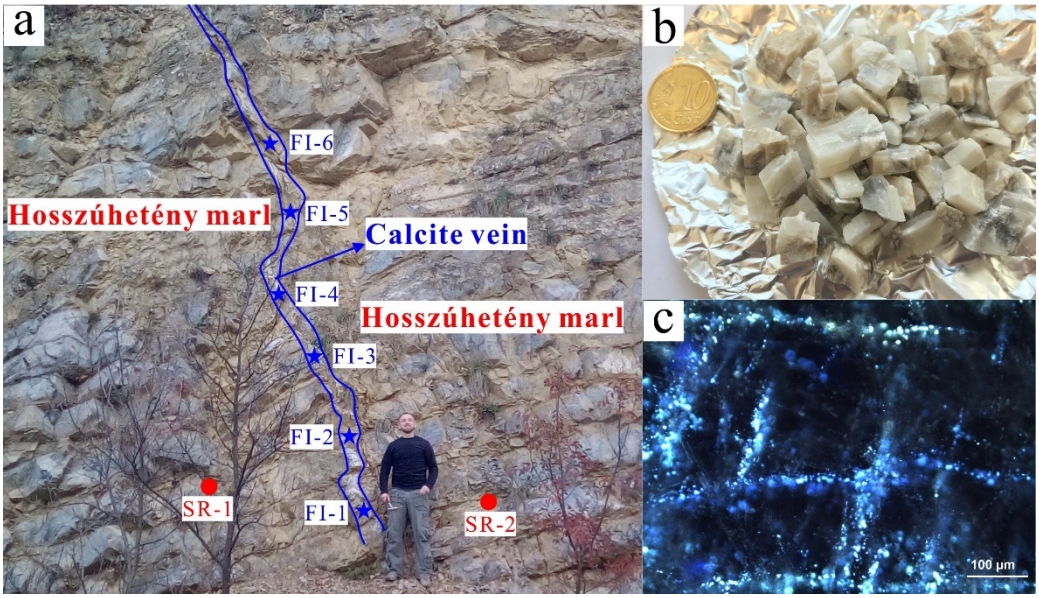

Fig. 2. Sample material: a) Calcite vein (marked with a blue line) filling a HCMF fracture. Blue stars represent calcite host mineral (FI) and red dots source rock (SR) sampling positions. b) Calcite vein material from the HCMF fracture. c) Photomicrograph of fluid inclusion trails under UV light showing the presence of petroleum by pale-blue and yellowish-blue fluorescence.

3 Methods

3.1 Sample preparation

Two powdered marl SR samples (SR-1 and SR-2) were extracted by a mixture of

184 dichloromethane (DCM) and methanol (99:1, v/v) at 50 °C using Soxhlet extraction
185 for 24 h, the extracts termed SR extracts. Six calcite crystal concentrates (FI-1 to FI-6)
186 were cleaned using the rigorous clean-up protocols developed by Han et al. (2020). In
187 brief, host minerals were washed with a Waller solution containing 33% sodium
188 dithionite, 28% sodium bicarbonate, 59% sodium citrate in distilled water. Then the
189 host minerals were transferred into a Soxhlet extraction thimble and washed twice (24
190 h) with DCM mixed with methanol (99:1, v/v) at 50 ℃. Afterwards, the minerals
191 were washed with three different organic solvents in the following order: methanol,
192 blend of dichloromethane (DCM) and methanol (93:7, v/v), and DCM. The DCM
193 extract from the last cleaning step was collected and residual particles were removed
194 using a pre-cleaned thimble. This DCM extract was used as procedural blank for the
195 respective sample. Before continuing, the procedural blanks were measured by GC-
196 MS and FT-ICR-MS and controlled for the amounts of remaining bitumen. The
197 washing procedure of the calcites was repeated until the cleaning of the outer mineral
198 surfaces from bitumen residues was deemed successful. Afterwards the cleaned
199 calcite crystals were crushed in a small metal cylinder with two stainless steel balls,
200 and finally, the inclusion oil (named as FI oil) in the powdered sample was extracted
201 by a mixture of DCM and methanol (99:1, v/v) using Soxhlet extraction.

202 The source rock extracts (SR-1 and SR-2) were split into two parts: one for GC-
203 MS and GC-IRMS analyses and the other for FT-ICR-MS analysis. Due to the fact
204 that only low amounts of FI oils were anticipated, the six FI oil samples from the
205 HCMF calcite vein were divided into two sets: FI-1 and FI-2 were used for GC-MS

and GC-IRMS analyses, and FI-3 to FI-6 were used for FT-ICR-MS analysis. The extracts for FI-1 and FI-2 were deasphaltened to obtain the *n*-hexane-soluble maltene fraction. Subsequently, the maltenes were further separated into aliphatic, aromatic and NSO-compound fractions using a medium pressure liquid chromatography (MPLC) system (Radke et al., 1980). The extracts FI-3 to FI-6 were analysed directly by FT-ICR-MS with no prior treatment.

3.2 Microscopy

FI analysis was conducted on doubly polished thick sections, with thickness of 130–150 μm to ensure the transparency of the calcite in transmitted light. Oil FIs were studied in reflected light using an Olympus UV lamphouse with a USH-1030L 100W mercury lamp connected to the BX50 Olympus microscope, and long-working distance objectives with various magnifications (5×, 10×, 20×, 50×).

3.3 GC-MS

The aliphatic and aromatic fractions of two SR extracts (SR-1 and SR-2) and two FI oils (FI-1 and FI-2) were selected for GC-MS analysis using a Trace GC Ultra coupled to a DSQ mass spectrometer (Thermo Electron Corp.). The Agilent 6890 Series GC instrument was equipped with a Thermo PTV injection system and a SGE BPX5 fused silica capillary column (50 m × 0.22 mm ID and 0.25 μm film thickness). Helium was used as a carrier gas. The GC oven was programmed from 50 to 310 °C at a rate of 3 °C/min, followed by an isothermal phase of 30 min. The MS was operated in electron impact ionization mode (EI) at 70 eV. Full scan mass spectra for compound identification were recorded from *m/z* 50 to 600 Da in the aliphatic fraction,

and from 50 to 330 Da in the aromatic fraction at a scan rate of 2.5 scans/second. In addition to the full scan mode, aliphatic fractions were also measured in the SIM (single ion monitoring) mode to improve the sensitivity for specific biomarkers such as hopanes (*m/z* 191) and steranes (*m/z* 217).

3.4 GC-IRMS

The *n*-alkanes in the aliphatic fraction of the two source rock extracts (SR-1 and SR-2) and the combined FI oils (FI-1 and FI-2) were analyzed by GC-IRMS using a GC unit (7890N, Agilent Technology, USA) connected to a GC-Isolink that is coupled via open split with a Delta V Plus mass spectrometer (ThermoFisher Scientific, Germany). For carbon isotope analysis, the organic compounds of the GC effluent stream were oxidized to CO_2 on a CuO/Ni/Pt catalyst in the combustion furnace held at 940 °C. 3 µl of saturated fraction were injected to the injector, working in splitless mode and held at a constant temperature of 300 °C. The aliphatic fractions were separated on a fused silica capillary column (HP Ultra 1, 50 m × 0.2 mm ID, 0.33 µm FT, Agilent Technology, Germany). The temperature program started at 80 °C, held for 2 minutes. Temperature was increased at a rate of 5 °C min^{-1} to 320 °C and with a lower rate of 1 °C min^{-1} increased to 325 °C, which was held for 15 minutes. Helium, set to a flow rate of 1.3 ml min^{-1}, was used as carrier gas. All aliphatic hydrocarbon fractions were measured in triplicate and the standard deviation was ≤ 0.5‰ for most of the compounds. The quality of the isotope measurements was checked regularly by measuring different *n*-alkane standards with known isotopic composition (provided by Campro Scientific, Germany and Arndt Schimmelmann, Indiana University, USA).

3.5 FT-ICR-MS

Two SR extracts (SR-1 and SR-2) and four FI oils (FI-3 to FI-6) were selected for FT-ICR-MS analysis. Samples were measured using a 12 Tesla Solarix FT-ICR-MS from Bruker Daltonik GmbH (Bremen, Germany) in APPI (+) mode, which can ionize mainly aromatic compounds of low-polarity (Huba et al., 2016a). A standard solution of the extract with a concentration of 1 mg/mL in a mixture of methanol and hexane (9:1, v/v) was diluted with the same solvent mixture to give a final concentration of 20 µg/mL. The solutions were injected into the APPI source at a flow rate of 20 µL/h using a syringe pump (Hamilton), where the analytes were ionized using a krypton lamp at 10.6 eV. The instrumental parameters on APPI (+) mode were as follows: dry gas (N_2) flow rate 3 L/min and temperature 210 °C, nebulizing gas (N_2) 2.3 bar, capillary voltage 1000 V, additional collision-induced dissociation voltage of 30 V, ions accumulation time 0.03 s, transfer time 1 ms, 4 megaword data sets. A total of 300 mass spectra were accumulated in a mass range from *m/z* 147 to 1200.

In each spectrum, signals with a signal-to-noise ratio ≥ 8 were included into the further data assessment. Formula assignment was done using the isotopes ^{1}H, ^{12}C, ^{13}C, ^{14}N, ^{16}O, and ^{32}S, with the upper thresholds N ≤ 2, O ≤ 8, and S ≤ 2; C and H were unlimited. If no chemical formula within the allowed mass error of 0.5 ppm was found, the peak was not included into the mass/formula list. For each $C_cH_hN_nO_oS_s$ compound, its double bond equivalent (DBE) value was obtained by calculating DBE = c – h/2 + n/2 + 1, where c is carbon number, h is hydrogen number and n is nitrogen

number. Each DBE refers to the number of unsaturation or rings in the individual compound structure (Poetz et al., 2014).

4 Results

4.1 Microscopic characterization

Calcites from the investigated HCMF marl fracture host numerous oil inclusions, occurring in clusters and along trails cross-cutting the host mineral crystals, and with lengths less than 20 μm. The FI can be classified as secondary fluid inclusions which were trapped along a healed fracture (Goldstein and Reynolds, 1994). The oil FIs show mainly pale-blue and yellowish-blue fluorescence under UV light microscopy (Fig. 2c). According to a previous study investigating the FIs in the calcites from the HCMF by UV-fluorescence microspectroscopy (Lukoczki et al., 2012), there was no significant difference between the oil FIs of pale-blue and yellowish-blue fluorescent colors, indicating that the FI oils derive from the same fluid and that the variation in fluorescent colors of the present oil inclusion trails was not caused by maturity differences, but presumably by oil fractionation during trapping.

4.2 Biomarkers

Mass trace chromatograms of the hopanes (*m/z* 191) and steranes (*m/z* 217) from the SR extracts and the two FI oils FI-1 and FI-2 are shown in Fig. 3. All biomarker ratios quoted in this study were calculated from SIM data (Table 1). 18α(H)-trisnorneohopane (Ts) and C_{30} αβ-hopane or 18α(H)-30-norneohopane (C_{29}Ts) are the most abundant hopanes in both SR extracts and FI oils investigated. The C_{31} αβ-22S/(22S + 22R) hopane values (~ 0.59) are very similar in SR extracts and FI oils.

The significant presence of C_{35} homohopanes can be seen in Fig. 3 and the respective C_{35} homohopane index data are listed in Table 1.

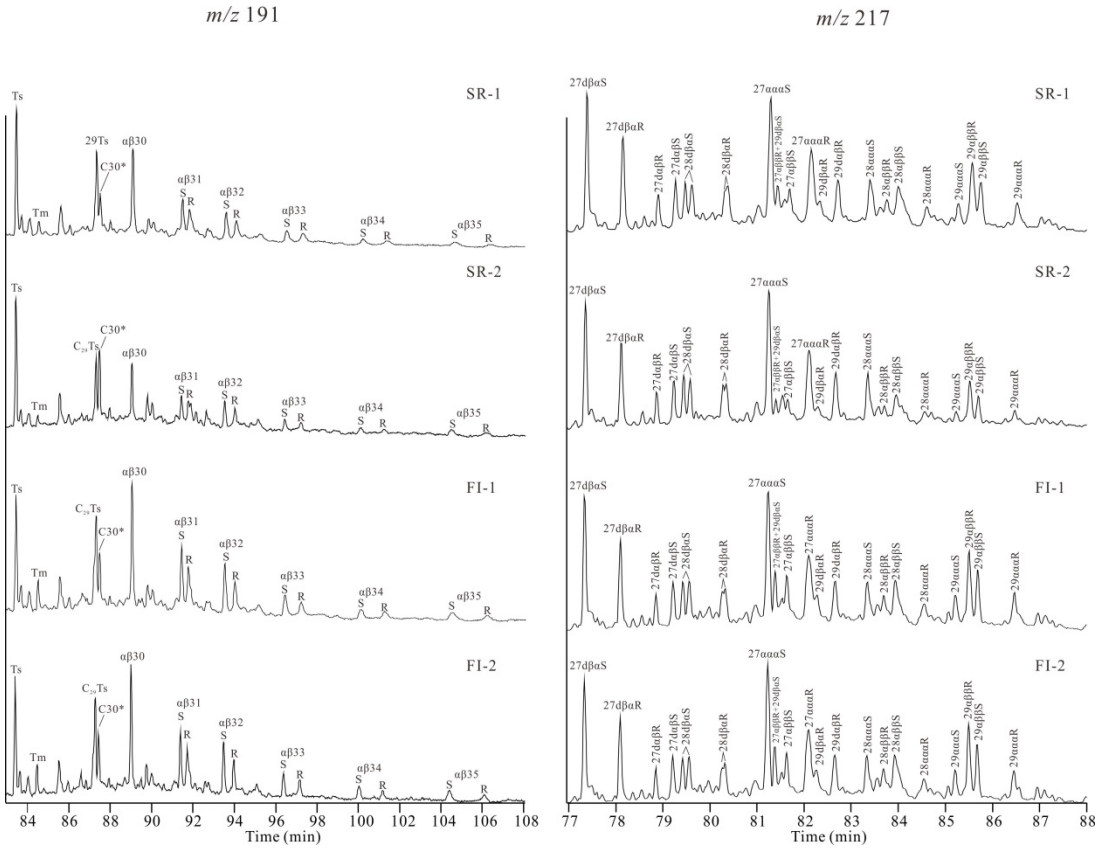

Fig. 3. Comparison of the hopane (*m/z* 191) and sterane (*m/z* 217) mass traces of the two source rock (SR) extracts SR-1 and SR-2 and the two fluid inclusion (FI) oils FI-1 and FI-2 from the HCMF marl in the Mecsek Mountains, Hungary. Ts = 18α(H)-trisnorneohopane; Tm = 17α(H)-trisnorhopane; C_{29}Ts = 18α(H)-30-norneohopane; C_{30}* = 17α(H)-diahopane.

The SR extracts and FI oils show quite similar sterane and diasterane distributions, in which the C_{27} steranes and diasteranes are more abundant than the C_{28} and C_{29} congeners. The C_{29} ααα-20S/(20S + 20R) sterane ratios show similar values (~ 0.42) in SR extracts and FI oils (Fig. 3). In contrast, the C_{29} αββ/(αββ + ααα) sterane ratios and diasteranes/steranes ratios in SR extracts are slightly higher than in FI oils. One further difference is that SR extracts contain more steranes, relative to the

307 hopanes, than the FI oils.

308 Table 1. Aliphatic and aromatic hydrocarbon parameters for the two fluid inclusion (FI) oils FI-1
309 and FI-2 and source rock (SR) extracts SR-1 and SR-2 from the HCMF marl in the Mecsek
310 Mountains, Hungary.

Parameters	SR-1	SR-2	FI-1	FI-2
Hopanes/Terpanes				
Ts/(Ts + Tm)	0.79	0.9	0.77	0.79
C_{29}Ts/C_{29} αβ hopane	0.72	0.87	0.74	0.76
22S/(22S + 22R)	0.59	0.59	0.59	0.58
C_{35} homohopane index	0.12	0.15	0.12	0.15
Steranes				
20S/(20S + 20R)	0.42	0.40	0.42	0.43
ββ/(ββ + αα)	0.69	0.71	0.65	0.65
C_{27}/C_{29} sterane	3.25	5.22	2.27	2.48
Diasteranes/steranes	0.73	0.72	0.64	0.63
Steranes/17α(H)-hopanes	1.21	1.46	1	1.08
Aromatics				
MPI-1	0.58	0.57	0.57	0.58
Calculated Rc (%)	0.75	0.74	0.74	0.75

311 Note: Ts = 18α(H)-trisnorneohopane; Tm = 17α(H)-trisnorhopane; C_{29}Ts = 18α(H)-30-
312 norneohopane; 22S/(22S + 22R) = C_{31} αβ-22S/(22S + 22R) hopanes; C_{35} homohopane index =
313 C_{35}/(C_{31}–C_{35}) homohopanes; 20S/(20S + 20R) = C_{29} ααα-20S/(20S + 20R) steranes; ββ/(ββ + αα)
314 = C_{29} αββ/(αββ + ααα) steranes; C_{27}/C_{29} sterane = C_{27} ααα-20R/C_{29} ααα-20R sterane;
315 diasteranes/steranes = C_{27} βα-diasteranes/C_{27} (ααα + αββ) steranes; steranes/17α(H)-hopanes =
316 C_{27}–C_{29} steranes/C_{29}–C_{35} 17α(H)-hopanes; methylphenanthrene index (MPI-1) = 1.5 × (3MP +
317 2MP)/(P + 9MP + 1MP); calculated vitrinite reflectance (Rc) = 0.6 × MPI-1 + 0.4 (for 0.65% < Ro
318 < 1.35%; Radke and Welte, 1983).

319 Aromatic compounds such as phenanthrene, alkylphenanthrenes and
320 alkyldibenzothiophenes are also present in the two SR extracts and the two selected FI
321 oils. The distribution pattern of aromatic hydrocarbons changes with an increasing

degree of maturation (Radke and Welte, 1983) and thus, provides indication on the maturity level of the respective sample. Here, the phenanthrene maturity ratios such as MPI-1 and calculated vitrinite reflectance (Rc) point to similar maturity stages for the two SR and FI oil samples in accordance to the sterane maturity indices (Table 1).

4.3 Stable carbon isotopes

In Fig. 4 the $\delta^{13}C$ values of the *n*-alkanes from the two SR extracts (SR-1 and SR-2) and two FI oils (FI-1 and FI-2) are plotted against the carbon numbers. The $\delta^{13}C$ values of *n*-alkanes in SR extracts range from –32.8‰ to –35.4‰, which partly overlaps with the $\delta^{13}C$ values of the *n*-alkanes in the FI oils ranging from –31.1‰ to –34.1‰. In general, the SR extracts and FI oils show a similar variability in the isotopic compositions of *n*-alkanes; however, mainly long chain > C_{29} and to a smaller extent also short chain *n*-alkanes < C_{20} in SR extracts are slightly enriched in ^{13}C compared to those in the FI oils.

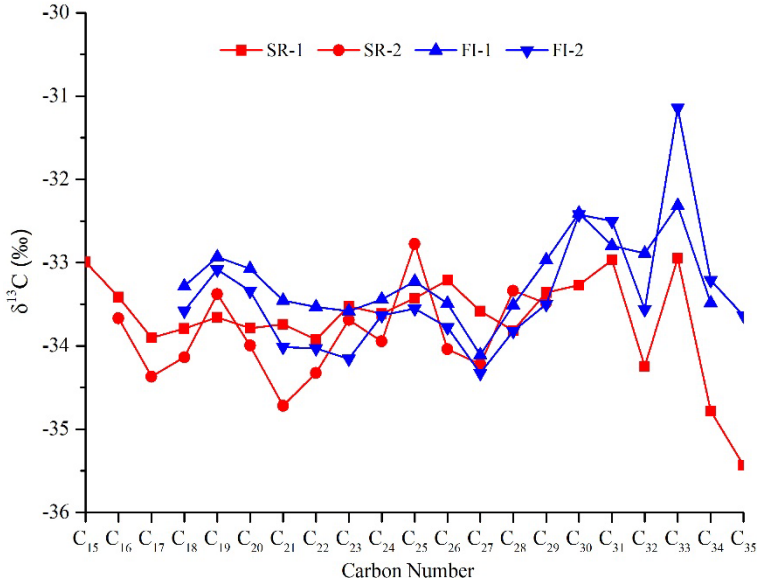

Fig. 4. Compound specific carbon isotope compositions of the *n*-alkanes from the aliphatic fractions in the source rock extracts (SR, blue lines) and inclusion oils (FI, red lines) from the

HCMF marl in the Mecsek Mountains, Hungary.

4.4 General characterization of hydrocarbons and NSO-compounds by FT-ICR-MS

Two SR extracts (SR-1 and SR-2) and four FI oils (FI-3 to FI-6) were characterized using FT-ICR-MS in APPI (+) mode. The abundances of individual compound classes show significant differences between the SR extracts and FI oils (Fig. 5). In the following, percentages of the total monoisotopic ion abundance (%TMIA) are used to express the relative abundances of compound classes (Hughey et al., 2002; Poetz et al., 2014). The aromatic HC class is the dominant compound group within both the FI oils (42.5% to 44 %TMIA) and SR extracts (34.1% to 41.8 %TMIA). The N_1 compound class shows a slightly higher abundance in the SR extracts (average value 15.8 %TMIA) compared to the FI oils (average value 12.1 %TMIA). In contrast, the O_1, N_1O_1 and S_1 compound classes show a stronger variability between FI oils and SR extracts. The O_1 class is the most abundant O_x class in all samples, showing a significant enrichment in the SR extracts (average value 17 %TMIA) compared to the FI oils (average value 12.5 %TMIA). The same trend can be observed for the N_1O_1 class with on average 7.2 %TMIA for the SR extracts and 2.9 %TMIA for the FI oils. In contrast, the S_1 compound class seems to exhibit an opposite trend with enrichment in the FI oils of on average 12 %TMIA compared to 7 %TMIA in the SR extracts. There is less difference within the O_2 class between SR extracts and FI oils (both ~ 5 %TMIA). The relative abundance of the remaining compound classes e.g., O_3, O_4, $N_1O_{2–8}$ and $S_1O_{2–8}$, are lower than

5 %TMIA and will, therefore, not be discussed here in detail.

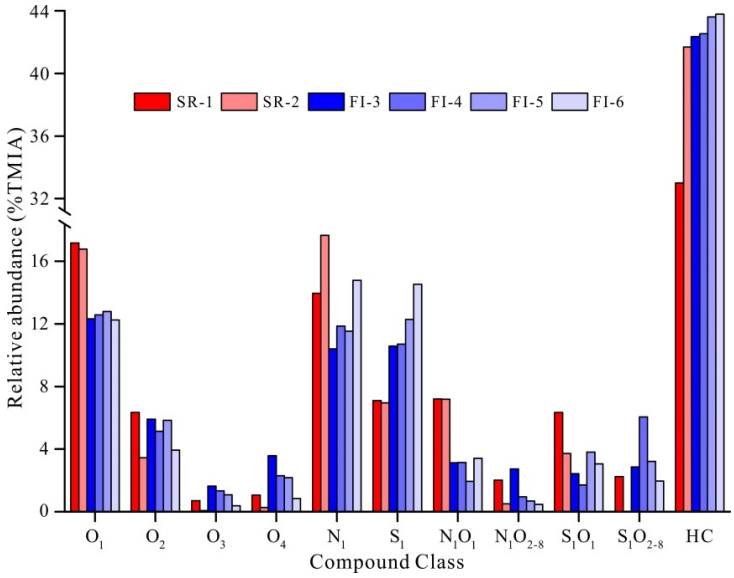

Fig. 5. Relative abundances of the main compound classes within the source rock (SR) extracts and fluid inclusion (FI) oils from the HCMF marl in the Mecsek Mountains (Hungary) measured by FT-ICR-MS in APPI (+) mode. HC = hydrocarbon.

Fig. 6 displays the mean DBE values and carbon numbers of all assessed compounds in the SR extracts and FI oils. The mean DBE values in the SR extracts (15.5 on average) are higher than those in the FI oils (11.2 on average) which suggests that compounds in the retained bitumen show a higher aromatic character and molecular size (larger ring system). The mean carbon numbers in SR extracts (38.4 on average) are similar to that in the FI oils (37.9 on average) implying that there is no preferential expulsion of compounds with a specific carbon number range.

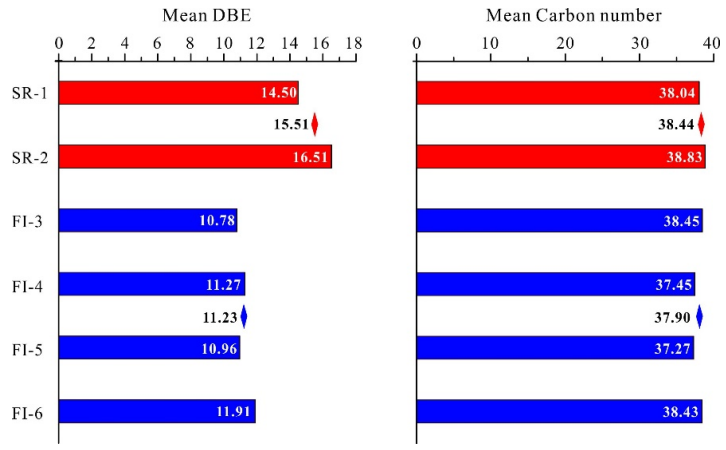

Fig. 6. Mean double bond equivalent (DBE) values and carbon numbers of all assessed compounds detected by FT-ICR-MS in APPI (+) mode in source rock (SR) extracts and fluid inclusion (FI) oils from the HCMF marl in the Mecsek Mountains, Hungary. Colored rhombus represents the average mean value of each sample type.

4.5 Compositional changes of individual compound class using FT-ICR-MS

In addition to the quantitative changes of individual compound classes presented above, the FT-ICR-MS technique allows compositional changes within the compound classes to be assessed with regard to their carbon number range and DBE distributions. Thus, in the following sections, the main compound classes (HC, S_1, O_1, O_2, and N_1) were described in more detail to reveal fractionation within each of these classes during primary oil migration. Here, the normalized abundance (%) within a DBE or carbon number distribution is expressed relative to the total monoisotopic ion abundance of each individual compound and DBE class, respectively.

4.5.1 HC compounds

The APPI (+) mode ionizes mainly aromatic HC compounds (DBE ≥ 4) with small amounts of non-aromatic cyclic compounds (Huba et al., 2016a). A closer look

into the HC DBE distribution (Fig. 7a) reveals that the HC species in the SR extracts cover a DBE range from 3 to 35 with a maximum at DBE 10 or 11, followed by a gradual decrease with an intermediate smaller maximum at DBE 20. In contrast, FI oils show a DBE range from 3 to 30 with a maximum at DBE 9 or 10, followed by a steep and asymptotic decrease (Fig. 7a).

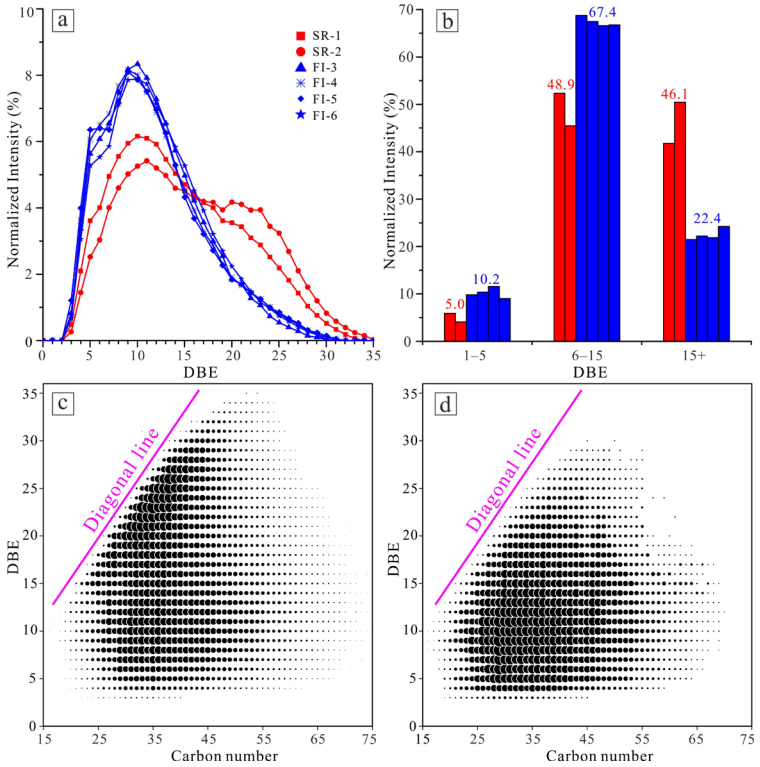

Fig. 7. a) Double bond equivalent (DBE) distributions of hydrocarbon (HC) in the two source rock (SR-1 and SR-2) extracts (red) and four fluid inclusion (FI-3 to FI-6) oils (blue). b) Normalized intensity of the low ($DBE_{1–5}$), medium ($DBE_{6–15}$) and high (DBE_{15+}) DBE groups of HCs in the SR extracts (red) and FI oils (blue) with numbers indicating average values. c) DBE versus carbon number plot of HCs in a representative SR extract (SR-2). d) DBE versus carbon number plot of HCs in a representative FI oil (FI-6). The normalized intensity (%) is expressed relative to the total monoisotopic ion abundance of the HC class. The magenta colored diagonal line delineates the minimum carbon number of a non-alkylated planar polycyclic aromatic core molecule within

every DBE class.

Based on their DBE values, the HC compounds are sorted into three groups, $DBE_{1–5}$, $DBE_{6–15}$ and DBE_{15+}, termed low, medium and high DBE compound groups, which represent compounds with different level of aromaticity and molecular size (the classification is the same for other compound classes described below). The relative abundances of the three HC DBE groups are plotted in Fig. 7b. The FI oils are dominated by the $DBE_{6–15}$ group (on average 67.4%) followed by the DBE_{15+} (on average 22.4%) and the $DBE_{1–5}$ (on average 10.2%) groups. The SR extracts consist of almost equal amounts of $DBE_{6–15}$ (on average 48.9%) and DBE_{15+} group (on average 46.1%) compounds. The $DBE_{1–5}$ group occurs only in relatively low abundance in the SR extracts (on average 5.0%). Obviously, the SR extracts are more enriched in DBE_{15+} compounds relative to the FI oils, while the FI oils contain a higher proportion of low and medium DBE group compounds. Moreover, HC compounds with high $DBE_{30–35}$ are absent in FI oils.

Looking into the carbon number distributions depicted by the DBE versus carbon number plots of one representative SR extract and one FI oil (Figs. 7c and 7d), the higher DBE classes (15–30) in the SR extract are dominated by compounds with carbon numbers between 25 and 45 close to a diagonal line which represents the minimum carbon number of a non-alkylated planar polycyclic aromatic core molecule within the respective DBE class. Compounds along this line are therefore aromatic compounds with a low degree of alkylation (Poetz et al., 2014; Mahlstedt et al., 2016). In contrast, the carbon number distributions in the FI oil per DBE class is shifted to

higher carbon numbers showing a Gaussian distribution maximizing at carbon number ranges that represent polycyclic aromatic compounds with medium alkylation degree.

4.5.2 S_1 compounds

The APPI (+) method is also sensitive for the ionization of organosulfur compounds from crude oil and sediment extracts (Purcell et al., 2006). S_1 compounds appear to be significantly more enriched in FI oils than in SR extracts (Fig. 5). The DBE distribution of the S_1 class in FI oils and SR extracts are significantly different (Fig. 8a). A bimodal DBE distribution with DBE values from 2 to 26 is displayed for the FI oils. The DBE distribution reveals two maxima: a smaller one at DBE 6 and a larger one at DBE 10. By comparison, the DBE values range from 6 to 31 in the SR extracts and show only one broad maximum between 12 and 23. The DBE $\geq$ 3 S_1 compounds are most likely aromatic compounds that bear a thiophene unit, while S_1 compounds with lower DBE number can be interpreted to represent alkyl thiolanes (tetrahydrothiophenes) or alkyl thianes (tetrahydrothiopyrans) (Liu et al., 2018).

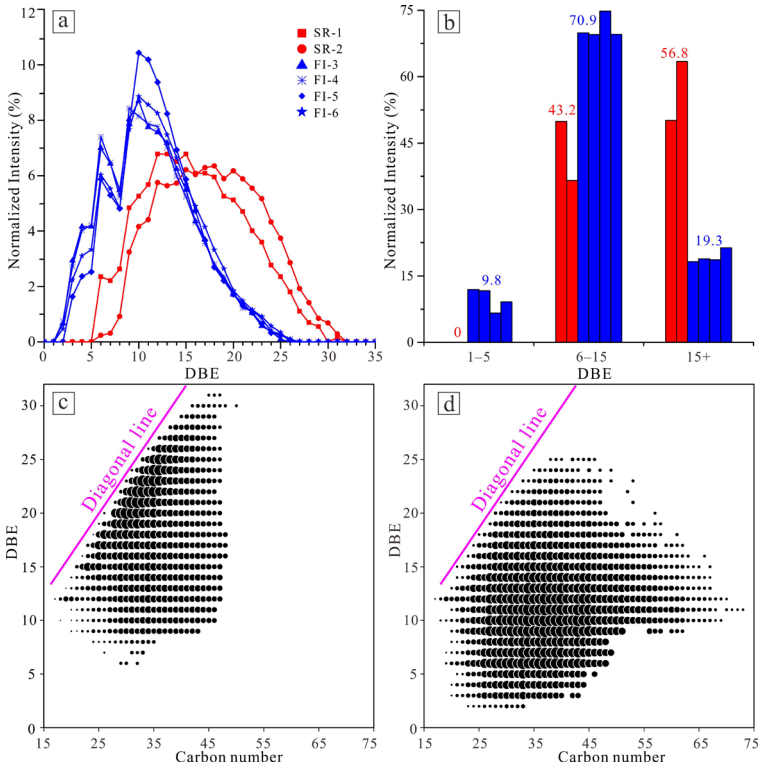

Fig. 8. a) Double bond equivalent (DBE) distributions of the S_1 compound class in the two source rock (SR-1 and SR-2) extracts (red) and four fluid inclusion (FI-3 to FI-6) oils (blue). b) Normalized intensity distribution of the three DBE groups $DBE_{1–5}$ (low), $DBE_{6–15}$ (medium) and DBE_{15+} (high) of S_1 class in the SR extracts (red) and FI oils (blue) with average value indicated. c) DBE versus carbon number plot of the S_1 class in a representative SR extract (SR-2). d) DBE versus carbon number plot of the S_1 class in a representative FI oil (FI-6). The normalized intensity (%) is expressed relative to the total monoisotopic ion abundance of the S_1 class. The magenta colored diagonal line delineates the minimum carbon number of a non-alkylated planar polycyclic aromatic core molecule within every DBE class. Note that S_1 compounds with carbon numbers above 50 in the SR extract are not included due to instrumental resolving power limitations for S_1 compounds in the here investigated SR sample (see text).

As for the HCs, the S_1 compounds are separated into three DBE groups. The SR extracts do not contain any $DBE_{1–5}$ S_1 compound, but significant proportions of

454 $DBE_{6–15}$ (on average 43.2%) and especially DBE_{15+} compounds (on average 56.8%).
455 In contrast, FI oils exhibit the highest content of $DBE_{6–15}$ compounds (on average
456 70.9%), and significantly lower amounts of DBE_{15+} S_1 compounds (on average
457 19.3%). $DBE_{1–5}$ S_1 compounds occur at least with an average share of 9.8%.
458 Comparing the two sample types, the low and medium DBE S_1 groups are dominant
459 in the FI oils, while the high DBE group is most abundant among the S_1 compounds
460 in the SR extracts. Moreover, S_1 compounds with DBEs from 27 to 31 are not
461 observed in the FI oils.

462 Looking into the DBE versus carbon number distributions of one representative
463 SR extract and one FI oil (Figs. 8c and 8d), the higher DBE classes (15–31) in the SR
464 extract are dominated by compounds with carbon numbers between 22 and 43 close to
465 the diagonal line, indicating a low alkylation degree of the polyaromatic system. In
466 contrast, the carbon number distributions in the FI oil are shifted to higher carbon
467 numbers showing a Gaussian distribution and thus a higher degree of alkylation of the
468 polyaromatic ring system. In the SR extract high molecular weight S_1 compounds
469 with carbon number above 50 are missing in all DBE classes. This is due to
470 instrumental limitation: the resolving power of the FT-ICR-MS instrument in the
471 broadband mode was in this case for the investigated complex SR sample too low to
472 separate the signal of the S_1 compounds from other compound groups in the high
473 molecular mass range, which has an impact on the abundance assessment of S_1
474 compounds in the SR samples. However, the fact that the main abundance of S_1
475 compound is located in the carbon number range close to the diagonal line (Fig. 8c)

476 and that the compound abundance significantly decreases with increasing carbon
477 numbers (especially >50) as confirmed by the other compound classes (Figs. 7c, 9c,
478 10c and 11c), suggests that S_1 compounds, despite of the detection limitation in the
479 SR samples, are preferentially expelled.

480 **4.5.3 O_1 compounds**

481 O_1 compounds detected in APPI (+) mode are suspected to be aliphatic and
482 aromatic aldehydes, alcohols, ketones and furans (Huba et al., 2016a). The O_1
483 compounds are the most abundant oxygen-containing compounds in both the SR
484 extracts and FI oils and the relative abundance of O_1 species is higher in the SR
485 extracts than in the FI oils (Fig. 5). The clear increase of oxygenated hydrocarbons in
486 crude oils with weathering has been reported by Huba et al. (2016b), but this is not the
487 case here since fresh HCMF marl samples were collected from abandoned quarry. For
488 the O_1 class, the SR extracts have a monomodal DBE distribution with DBE values in
489 the range between 1 and 32 (Fig. 9a). In comparison, the FI oils show a DBE
490 distribution between 1 and 27 DBE, and exhibit an odd-over-even carbon number
491 predominance in the DBE 1 to 9 range (except for sample FI-4) with a maximum at
492 DBE 1 and an additional maximum between DBE 10 and 15.

493 Fig. 9b exhibits the intensity distribution of the three classified DBE groups. The
494 FI oils are dominated by O_1 compounds in the $DBE_{6–15}$ group (on average 56.6%)
495 followed by O_1 compounds in the DBE_{15+} (on average 22.3%) and $DBE_{1–5}$ groups
496 (on average 21.1%). The SR extracts show high abundances of O_1 compounds within
497 the DBE_{15+} (on average 45.8%) and $DBE_{6–15}$ (on average 45.7%) groups followed by

compounds from the $DBE_{1–5}$ group (on average 8.5%). In comparison, the SR extracts are dominated by the medium and high DBE group compounds, while the FI oils are dominated by the medium DBE group compounds.

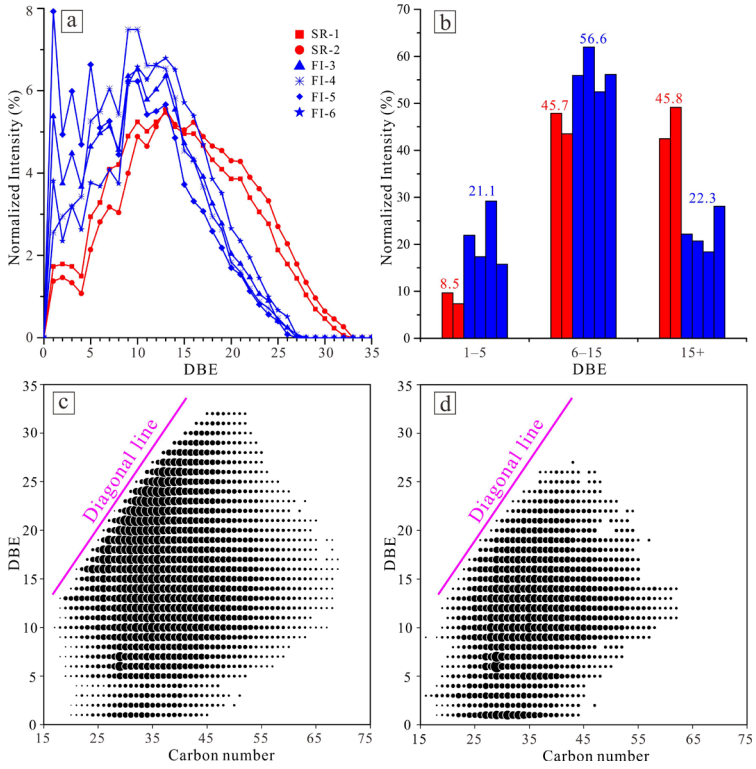

Fig. 9. a) Double bond equivalent (DBE) distributions of the O_1 compound class in the two source rock (SR-1 and SR-2) extracts (red) and four fluid inclusion (FI-3 to FI-6) oils (blue). b) Normalized intensity distribution of the three DBE groups $DBE_{1–5}$ (low), $DBE_{6–15}$ (medium) and DBE_{15+} (high) for the O_1 class in the SR extracts (red) and FI oils (blue) with average value indicated. c) DBE versus carbon number plot of the O_1 class in a representative SR extract (SR-2). d) DBE versus carbon number plot of the O_1 class in a representative FI oil (FI-6). The normalized intensity (%) is expressed relative to the total monoisotopic ion abundance of the O_1 class. The magenta colored diagonal line delineates the minimum carbon number of a non-alkylated planar polycyclic aromatic core molecule within every DBE class.

In the DBE versus carbon number plot the maximum of O_1 species in the

representative SR extract is also located close to the diagonal line with higher DBEs and lower carbon numbers (Fig. 9c). In contrast, in the FI oil O_1 compounds are more centered at lower DBE numbers: one center is in the DBE range from 9 to 18 and carbon numbers in the range between 20 and 50 and another center is in the DBE range from 1 to 6 and carbon numbers ranging from 20 to 40 (Fig. 9d).

4.5.4 O_2 compounds

The O_2 compounds are the second abundant oxygen class (Fig. 5). O_2 compounds detected in ESI (–) mode are regarded as tools to assess the level of biodegradation (Kim et al., 2005; Hughey et al., 2007). However, in APPI (+) mode they are not well studied, and they could be mixed aliphatic and aromatic dialdehydes, dialcohols, diketones and difurans or carboxylic acids (Huba et al., 2016a). The FI oils have a monomodal DBE distribution with DBE values in the range between 1 and 22, with a maximal relative abundance at DBE 2. The SR extracts show a wider DBE range from 2 to 28 and there is no apparent predominance of certain DBEs (Fig. 10a).

The FI oils show high relative O_2 compound abundances in the $DBE_{1–5}$ (on average 52.0%) and $DBE_{6–15}$ groups (on average 39.8%) followed by the DBE_{15+} group (on average 8.2%). In contrast, the SR extracts show highest abundance in the DBE_{15+} (on average 46.4%) and $DBE_{6–15}$ (on average 43.6%) groups and low abundance in the $DBE_{1–5}$ group (on average 10.1%) (Fig. 10b). Interestingly, all of the DBE 1 compounds are absent in SR extracts but present in FI oils. Moreover, DBE 2 compounds are very dominant in FI oils in contrast to the SR extracts (Fig. 10a).

The DBE versus carbon number plots indicate that high molecular weight

compounds from C_{16} to C_{54} with higher DBEs ranging from 2 to 29 are preferentially present in the SR extract (Fig. 10c), while high molecular weight O_2 compounds ranging from C_{16} to C_{52} with low DBEs from 2 to 8 are preferentially found in the FI oil (Fig. 10d).

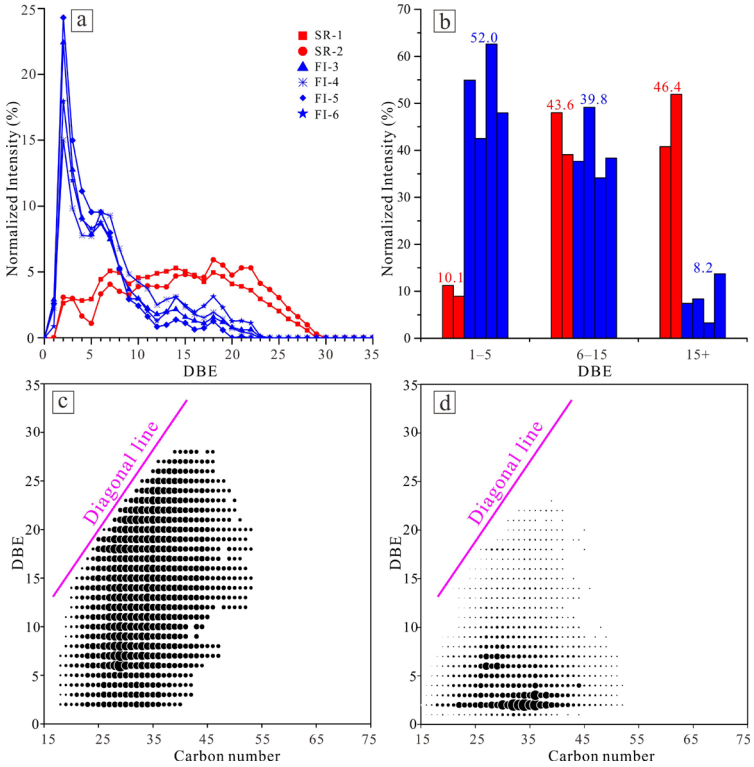

Fig. 10. a) Double bond equivalent (DBE) distributions of the O_2 compound class in the two source rock (SR-1 and SR-2) extracts (red) and four inclusion (FI-3 to FI-6) oils (blue). b) Normalized intensity distribution of the three DBE groups $DBE_{1–5}$ (low), $DBE_{6–15}$ (medium) and DBE_{15+} (high) for the O_2 class in SR extracts (red) and FI oils (blue) with average value indicated. c) DBE versus carbon number plot of the O_2 class in a representative SR extract (SR-1). d) DBE versus carbon number plot of the O_2 class in a representative FI oil (FI-3). The normalized intensity (%) is expressed relative to the total monoisotopic ion abundance of O_2 class. The magenta colored diagonal line delineates the minimum carbon number of a non-alkylated planar polycyclic aromatic core molecule within every DBE class.

548 **4.5.5 N_1 compounds**

549 Both pyrrolic (with nitrogen in a five-membered ring) and pyridinic (with
550 nitrogen in a six-membered ring) compounds can be ionized and identified by APPI
551 (+) mode (Marshall and Rodgers, 2008). The relative ion abundances of the N_1
552 compounds are quite variable between the two SR extracts but especially among the
553 FI oils. Overall, N_1 compound abundance might be a bit higher in the SR extracts
554 than in the FI oils (Fig. 5). However, there are significant differences within the DBE
555 distributions (Fig. 11a). Both show a monomodal distribution, but in the FI oils the
556 DBEs range from 5 to 27 with a maximum around DBE 12 and in the SR extracts
557 DBEs range from 7 to 34 with a maximum around DBE 19 or 21.

558 A closer look into the three classified DBE groups (Fig. 11b) shows that the FI
559 oils are dominated by N_1 compounds in the $DBE_{6–15}$ group (on average 63.6%),
560 followed by the DBE_{15+} group (on average 36.3%) and only very low amounts in the
561 $DBE_{1–5}$ (on average 0.1%) group. The SR extracts are dominated by N_1 compounds
562 in the DBE_{15+} group (on average 67.9%) followed by the $DBE_{6–15}$ group (on average
563 32.1%). As already seen for the other compound classes also the N_1 compounds in the
564 SR extracts show their highest proportion in the DBE_{15+} class while in the FI oil the
565 $DBE_{6–15}$ class is the most abundant. Also, the predominance of N_1 compound in the
566 SR extract in the DBE versus carbon number plot is shifted close to the diagonal line
567 in the higher DBE range (Fig. 11c). Generally, high $DBE_{28–34}$ compounds are only
568 retained in SR and are not expelled. In contrast, the DBE versus carbon number
569 distribution in the FI oil show a Gaussian distribution shifted to higher carbon

numbers and maximizing at carbon number ranges similar to HC class (Fig. 11d).

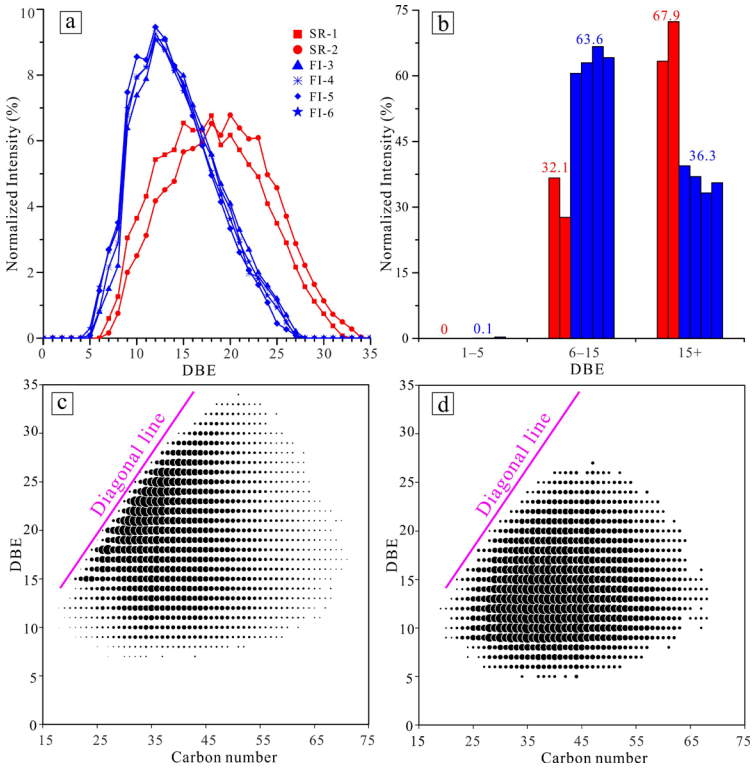

Fig. 11. a) Double bond equivalent (DBE) distributions of the N_1 compound class in the two source rock (SR-1 and SR-2) extracts (red) and four inclusion (FI-3 to FI-6) oils (blue). b) Normalized intensity distribution of the three DBE groups $DBE_{1–5}$ (low), $DBE_{6–15}$ (medium) and DBE_{15+} (high) for N_1 class in SR extracts (red) and FI oils (blue) with average value indicated. c) DBE versus carbon number plot of the N_1 class in a representative SR extract (SR-2). d) DBE versus carbon number plot of the N_1 class in a representative FI oil (FI-6). The normalized intensity (%) is expressed relative to the total monoisotopic ion abundance of the N_1 class. The magenta colored line represents the diagonal line indicating the minimum carbon number of a non-alkylated planar polycyclic aromatic core molecule within every DBE class.

5 Discussion

5.1 Correlation of SR extracts and FI oils by facies biomarkers, maturity indicators and stable carbon isotopes

584 Hopanes and steranes were widely used for tracing facies differences and
585 similarities of the SR extracts and FI oils (Peters et al., 2005). High steranes/17α(H)-
586 hopanes ratios in both SR extracts and FI oils reflect an origin of marine organic
587 matter (OM) with major contributions from planktonic and/or benthic algal material
588 (Moldowan et al., 1985; Peters et al., 2005). The predominance of C_{27} steranes and
589 the significant amount C_{35} homohopane suggests OM with a high proportion of
590 microalgae deposited in dysoxic to anoxic environments (Moldowan et al., 1985;
591 Peters and Moldowan, 1991). High diasteranes/steranes ratios commonly indicate
592 clay-rich source rocks (Peters et al., 2005), while the reverse can be observed in some
593 organic-lean carbonate rocks (Clark and Philp, 1989). The diasteranes/steranes values
594 of the SR extracts are in accordance with their marly lithofacies typical for calcareous
595 deposits with a distinct clay content (Clark and Philp, 1989). Overall, the source-
596 related parameters suggest that the FI oils are derived from SRs deposited under
597 anoxic marine environmental conditions, which is in agreement with a previous study
598 showing that HCMF marl was deposited in an open marine, relatively deep basin
599 (Raucsik, 2012c).

600 Concerning their level of maturity both the SR extracts and FI oils are beyond
601 the early oil generation window, as indicated by similar C_{31} αβ-22S/(22S + 22R)
602 hopane ratios having reached its equilibrium (0.59) (Seifert and Moldowan, 1980).
603 The similar C_{29} ααα-20S/(20S + 20R) sterane ratios confirm the similar maturity
604 stages of SR extracts and FI oils. The same is true for the Ts/(Ts + Tm) ratios,
605 although the value of SR-1 is lower than SR-2 which might reflect some

compositional heterogeneity in the source rock facies. However, the C_{29} αββ/(αββ + ααα) sterane ratios are equivocal, exhibiting slightly higher maturity levels for the SR extracts than for the FI oils. The maturity-related parameters can be affected by source OM input (Peters et al., 2005), but FI oils should have been derived from the same source rock deposited under similar marine environmental conditions. Fractionation induced by oil migration has also been debated for steranes and hopanes for long time (Seifert and Moldowan, 1981; Han et al., 2017), which can lead to different sterane and hopane ratios in expelled fluids compared to the retained bitumen. In addition to the hopane and sterane derived maturity parameters, further thermal maturity information can be gained from the phenanthrene maturity ratios, which are not affected by expulsion fractionation (Leythaeuser et al., 1988c). The substantially identical Rc values suggest that the maturity of FI oils and SR extracts is similar. Thus, although there are some individual variabilities in the biomarker maturity parameters, most parameters indicate equal maturation stages for the SR extracts and the FI oils.

The stable carbon isotopic compositions of the *n*-alkanes are useful for oil-source correlations, since the *n*-alkane isotope signatures of a crude oil are primarily controlled by the OM input (Sofer et al., 1984; Bjorøy et al., 1994; Murray et al., 1994). Fig. 4 exhibits that the carbon isotopic signatures of *n*-alkanes in the SR extracts and FI oils are essentially in the same range, which points to an origin of the FI oils trapped in calcite veins from HCMF marl SRs. However, the increasing deviation of the carbon isotopic compositions in the long chain *n*-alkane range (> C_{29}) of the SR extracts and the FI oils (Fig. 4) might be caused by isotopic fraction that is

628 induced by thermal maturation or migration during the generation and expulsion
629 process (Sofer et al., 1984; Tissot and Welte, 1984; Clayton, 1991; Dzou and Hughes,
630 1993; Cramer et al., 1998; Liao and Geng, 2009). Since the thermal maturation of
631 both SR extracts and FI oils has been shown to be in a similar range, it is suggested
632 that the slightly heavier $\delta^{13}C$ signal of especially the long chain *n*-alkanes in the
633 expelled oils (FI oils) is the result of fluid migration. Higher molecular weight HCs in
634 the migrating fluids are preferentially adsorbed onto mineral surfaces (Schwark et al.,
635 1997; George et al., 1998) and it is suggested that such a preferential adsorption also
636 leads to a slight isotopic fractionation with an enrichment of heavier *n*-alkanes in the
637 FI oils.

638 Thus, based on the biomarker parameters and carbon isotope signatures
639 presented here, the HCMF marl SRs correlate very well with the investigated FI oils.
640 In consequence, it can be assumed that when the HCMF reached the oil window, oil
641 expulsion occurred and the expelled oil was trapped in pre-formed calcite veins as
642 secondary inclusions (Fig. 2c). These FI oils are suggested to preserve the original
643 information of the expelled fluids from the HCMF marl. Due to the similar maturity
644 levels between SR extracts and FI oils, the maturity of Rc 0.74% can be regarded as
645 the onset of oil expulsion from the HCMF marl, otherwise the maturity level in the FI
646 oils, representing early oil expulsion, should be lower than in the SR extracts.
647 Although a bit higher, the onset of oil expulsion for HCMF marl is in the same range
648 as other source rocks such as the Posidonia shale with a vitrinite reflectance (Ro) of
649 0.68% (Rullkötter et al., 1988; Mahlstedt et al., 2016) and the North Sea Spekk shale

650 at a vitrinite reflectance equivalent (VRE) of 0.7% (Heum et al., 1986).

651 5.2 Compositional fractionation during primary migration revealed 652 by FT-ICR-MS

653 The organic components distributed throughout a marl can be variably
654 partitioned between the oil and brine phases, and the carbonate and clay mineral
655 surfaces (Mann et al., 1997). It is suggested that the migration behavior can depend on
656 the functional group and its polarity, shielding effects concerning the functional group
657 due to specific molecular configurations (e.g. alkyl branches) and on the molecular
658 shape (e.g., aromatic system etc.) and size (Li et al., 1995; Larter et al., 1996; Poetz et
659 al., 2014, 2020; Mahlstedt et al., 2016; Han et al., 2018a, 2018b; Yue et al., 2021).

660 5.2.1 Fractionations of different compound classes

661 O_1, N_1, N_1O_1 and S_1O_1 compounds are relatively enriched in the HCMF marl
662 SR extracts when compared to the FI oils (Fig. 5), suggesting that these compound
663 classes are preferentially retained in the SRs being at the onset of oil expulsion (Rc ~
664 0.74%). The HC class is the most dominant class in the SR extracts and especially in
665 the FI oils (Fig. 5). The relative abundance of the HC class in the SR extracts is quite
666 variable, which points to some heterogeneity within the source rock unit. However, if
667 the average relative abundance of HC in the SR extracts is compared to that of the FI
668 oils, a preferential expulsion is suggested. The S_1 compounds appear to be more
669 abundant in the FI oils, pointing to an overall preferential expulsion of these
670 compounds. O_2 compounds seem to show no preference. These differences are
671 suggested to be the expression of different adsorption affinities of these different

functional groups (e.g., hydroxy, carbonyl, carboxyl, pyrrolic, carbazolic, thiophenic and thiol groups), on mineral surfaces in the oil-water-rock system (Larter and Aplin, 1995; Adams, 2014). Previous experiment and computer simulation studies have revealed that oxygen- and particularly nitrogen-containing compounds exhibit a higher adsorption affinity onto surfaces than sulfur-containing compounds, since sulfur represents a significantly weaker dipole (López-Linares et al., 2006; González et al., 2007; Adams, 2014; Ataman et al., 2016). In addition to this, the acidic and alkalinic character of functional groups are suggested to affect the adsorption process (Drummond et al., 2004; Adams, 2014). For instance, experimental work suggested that pyridinic nitrogen compounds preferentially adsorb on mineral surfaces compared with pyrrolic compounds (Reed, 1968; Larter and Aplin, 1995). Besides that, source rocks comprise organic and inorganic materials containing various active sites that significantly interact with functional groups in oil constituents (Stanford et al., 2007). For example, Yue et al. (2021) showed that N_y and N_yO_x compounds are preferably retained in the biogenic carbonate-rich Barnett and biogenic quartz-rich Niobrara shale (USA) compared with other compound classes.

5.2.2 Effect of compound aromaticity on compositional fractionations

The assessment of the quantitative fractionation of different compound classes provides a first insight into the expulsion and retention behavior of these compound classes with respect to their functional groups. However, a deeper view into the component inventory of the different compound classes show significant differences in the compound composition with regard to DBE and carbon number when

694 comparing SR extracts and FI oils.

695 To visualize those compositional differences, the abundances of three DBE
696 groups $DBE_{1–5}$ (low), $DBE_{6–15}$ (medium) and DBE_{15+} (high) are depicted in a
697 triangular plot in Fig. 12. The data clearly show that the bitumen retained in the SR is
698 enriched in HC, S_1, O_1, O_2 and N_1 compounds with a higher proportion of DBEs. In
699 contrast, the expelled fluid in the FI oils is enriched in respective compounds with a
700 low to medium content of DBEs. Thus, the data from the HCMF marl imply that
701 compounds with a higher aromaticity and due to the larger ring system a higher
702 molecular size are preferentially retained, while those with a low to medium
703 aromaticity and smaller molecular size are preferentially expelled. This finding is in
704 agreement with studies comparing reservoir and source rock units (Mahlstedt et al.,
705 2016; Han et al., 2018b; Yue et al., 2021), suggesting a preferential removal of
706 compounds with lower DBEs during primary migration, while compounds with
707 higher DBEs are preferentially retained in source rock. Moreover, compared to these
708 previous studies (Mahlstedt et al., 2016; Han et al., 2018b) which focused on the
709 nitrogen-containing compounds, the current results indicate that this preferential
710 behavior is also true for other compound classes. Former asphaltene (condensed
711 polyaromatic backbone strewn with heteroatoms) adsorption experiments and
712 computer simulations indicated that larger aromatic ring systems and thus increased
713 aromaticity allow surface active areas of heteroatoms to more favorably adsorb onto
714 surfaces (López-Linares et al., 2009; Marchal et al., 2010). For example, Plancher et
715 al. (1977) found that 5-aromatic ring structured compounds adsorbed more firmly to

mineral surfaces than 2-aromatic ring structured compounds. Additionally, Yue at al. (2021) showed that depending on the micropore size of the host rock, lower DBE species, representing smaller molecular sizes, migrate more easily out of the source rock compared with higher DBE species, resulting into the retention of these compounds in source rock. The same can be observed in this study for HCs and NSO-compounds with a higher degree of aromaticity (high DBEs) which are preferentially retained in the SRs. This deeper data evaluation shows that in addition to the functional group, structural properties play a major role for the fractionation behavior.

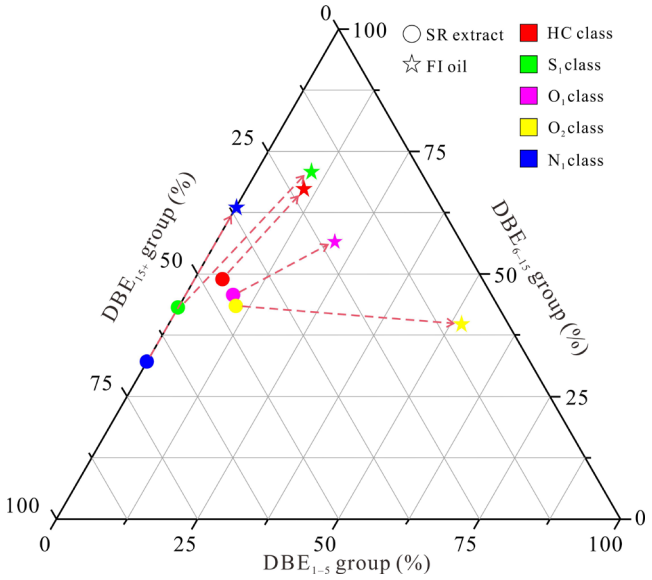

Fig. 12. Ternary diagram of three double bond equivalent (DBE) groups $DBE_{1–5}$, $DBE_{6–15}$ and DBE_{15+} for hydrocarbon (HC), S_1, O_1, O_2, N_1 classes in source rock (SR) extracts (with average value) and fluid inclusion (FI-6) oils (with average value) from the HCMF (Hungary). Red arrow indicates the compositional changes between SR bitumen and expelled oil.

5.2.3 Effect of alkylation degree on compositional fractionations

The degree of alkylation represents the length of alkyl side chains for a given compound class and/or DBE (Marshall and Rodgers, 2008). The shielding effect

induced by aliphatic side chains, that could reduce interactions with the mineral active sites, was considered to affect the retention capacity (Li et al., 1995; Larter et al., 1996; Mahlstedt et al., 2016; Yue et al., 2021). The FT-ICR-MS technique provides only information on the carbon number range (with regard to DBEs) and, therefore, maybe on the degree of alkylation, but gives no clue about the alkyl chain configuration within the molecule.

The carbon number range is in most cases similar for the retained and expelled compounds, with exception of the S_1 compounds but this distribution is impaired by compound assignment problems as discussed above (Fig. 8). However, the data show that compounds with higher DBEs in the SR extracts are more enriched in the lower carbon number range (low alkylated species) close to the diagonal line, which represents the minimum carbon number of a non-alkylated planar polycyclic aromatic core molecule within the respective DBE class (Figs. 7c, 8c, 9c, 10c and 11c). Fig. 13 exhibits the carbon number distribution of the representative DBE 12 (medium DBE range) and DBE 20 (high DBE range) classes of the N_1 and HC compounds in the SR extracts and FI oils. The medium DBE 12 class of the N_1 and HC compounds shows no preferential expulsion in terms of the carbon number (Fig. 13a). In contrast, in the higher DBE range (DBE 20) N_1 and HC compounds with less or shorter alkyl chains (lower carbon numbers) are preferentially retained in the SRs (Fig. 13b). This suggests that in these compounds the centers of increased interaction (hetero-atoms and aromatic rings) are less shielded by long alkyl chains in appropriate positions leading to their preferential retention in the SR.

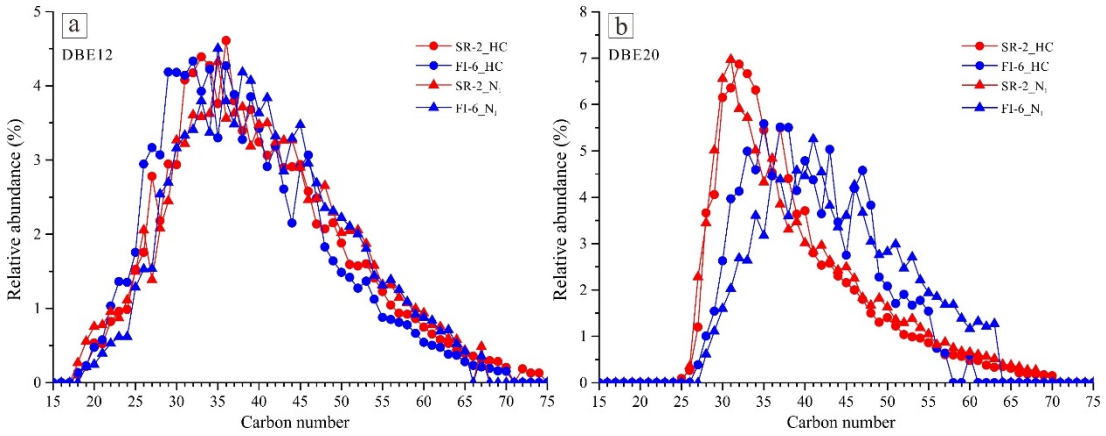

Fig. 13. Carbon number distributions of a) the DBE 12 and b) DBE 20 class of N_1 and HC compounds in a representative source rock (SR-2) extract and fluid inclusion (FI-6) oil from the HCMF (Hungary). The relative abundance in percent is expressed relative to the total ion abundance of compounds for the DBE distribution.

Thus, although the FT-ICR-MS cannot provide direct structural information, the DBE versus carbon number plot can give insight into the alkylation degree of the retained and expelled compounds. The observation that those high DBE compounds with a lower degree of alkylation are preferentially retained suggests that shielding effects play an additional role for the retention and expulsion of the petroleum constituents.

Conclusions

The biomarker and stable carbon isotope data indicate that the investigated FI oils trapped in a calcite vein comprise expelled fluids (Rc ~ 0.74%) from the adjacent HCMF marl source rock. On a functional group level the FT-ICR-MS measurements indicate that O_1, N_1, N_1O_1 and S_1O_1 compounds are preferentially retained in the source rock, while less polar compounds such as aromatic HC and S_1 compounds are

assumed to be preferentially expelled. A deeper insight into the compound inventory shows that HCs and NSO-compounds with higher aromaticity are preferentially retained in the source rock during primary migration, which is especially true for high DBE compounds in the lower carbon number range indicating a lower degree of alkylation and thus a less pronounced shielding effect. These findings confirm earlier work suggesting that functional groups, aromaticity and the alkylation degree of HCs and NSO-compounds are the main factors affecting compositional fractionation of petroleum during primary migration.

Acknowledgements

The China Scholarship Council (CSC) is gratefully acknowledged for funding Yufu Han's research. Sophie Müller-Moewes and the Center for Junior Scholars (CJS) from the Technical University Berlin are also thanked for supporting me with a Short-term scholarship for foreign students (STIBET) degree completion grant enabling me to finish my thesis. We thank the National Research, Development and Innovation Office (grant no. K-138919) from Hungary for supporting this study. We extend our gratitude to Cornelia Karger, Anke Kaminsky, Andrea Vieth-Hillebrand and Doreen Noack for their technical support. We also thank the editor Prof. Deolinda Flores and two anonymous reviewers for their careful and constructive reviews of this paper.

References

Adams, J.J., 2014. Asphaltene adsorption, a literature review. Energy Fuel 28, 2831–2856. https://doi.org/10.1021/ef500282p.

794 Ataman, E., Andersson, M.P, Ceccato, M., Bovet, N., Stipp, S.L.S., 2016. Functional group
795 adsorption on calcite: II. Nitrogen and sulfur containing organic molecules. J. Phys. Chem. C
796 120, 16597–16607. https://doi.org/10.1021/acs.jpcc.6b01359.
797 Bennett, B., Buckman, J.O., Bowler, B.F.J, Larter, S.R., 2004. Wettability alteration in petroleum
798 systems: the role of polar non-hydrocarbons. Pet. Geosci. 10, 271–277.
799 https://doi.org/10.1144/1354-079303-606.
800 Bjorøy, M., Hall, P.B., Moe, R.P., 1994. Stable carbon isotope variation of *n*-alkanes in Central
801 Graben oils. Org. Geochem. 22, 355–381. https://doi.org/10.1016/0146-6380(94)90114-7.
802 Bodnar, R.J., 1990. Petroleum migration in the Miocene Monterey Formation, California, USA:
803 constraints from fluid-inclusion studies. Mineral. Mag. 54, 295–304.
804 https://doi.org/10.1180/minmag.1990.054.375.15.
805 Burruss, R.C., 1981. Hydrocarbon fluid inclusions in studies of sedimentary diagenesis. In:
806 Hollister, L.S., Crawford, M.L. (Eds.), Fluid Inclusions: Applications to Petrology. Short
807 Course Volume, vol. 6. Mineral. Assoc., Canada, pp. 138–156.
808 Clark, J.P., Philp, R.P., 1989. Geochemical characterization of evaporite and carbonate
809 depositional environments and correlation of associated crude oils in the Black Creek Basin,
810 Alberta. Bull. Can. Petrol. Geol. 37, 401–416. https://doi.org/10.35767/gscpgbull.37.4.401.
811 Clayton, C.J., 1991. Effect of maturity on carbon isotope ratios of oils and condensates. Org.
812 Geochem. 17, 887–899. https://doi.org/10.1016/0146-6380(91)90030-N.
813 Clegg, H., Wilkes, H., Oldenburg, T., Santamaría-orozco, D., Horsfield, B., 1998. Influence of
814 maturity on carbazole and benzocarbazole distributions in crude oils and source rocks from
815 the Sonda de Campeche, Gulf of Mexico. Org. Geochem. 29, 183–194.

https://doi.org/10.1016/S0146-6380(98)00181-8.

Cobbold, P.R., Zanella, A., Rodrigues, N., Løseth, H., 2013. Bedding-parallel fibrous veins (beef and cone-in-cone): Worldwide occurrence and possible significance in terms of fluid overpressure, hydrocarbon generation and mineralization. Mar. Pet. Geol. 43, 1–20. https://doi.org/10.1016/j.marpetgeo.2013.01.010.

Cramer, B., Krooss, B.M., Littke, R., 1998. Modeling isotope fractionation during primary cracking of natural gas: a reaction kinetic approach. Chem. Geol. 149, 235–250. https://doi.org/10.1016/S0009-2541(98)00042-4.

Csontos, L., 1995. Tertiary tectonic evolution of the Intra-Carpathian area: a review. Acta Vulcan. 7, 1–13.

Csontos, L., Benkovics, L., Bergerat, F., Mansy, J.-L., Wórum, G., 2002. Tertiary deformation history from seismic section study and fault analysis in a former European Tethyan margin (the Mecsek-Villány area, SW Hungary). Tectonophysics 357, 81–102. https://doi.org/10.1016/S0040-1951(02)00363-3.

Drummond, C., Israelachvili, J., 2004. Fundamental studis of crude oil–surface water interactions and its relationship to reservoir wettability. J. Pet. Sci. Eng. 45, 61–81. https://doi.org/10.1016/j.petrol.2004.04.007.

Dzou, L.I., Hughes, W.B., 1993. Geochemistry of oils and condensates, K Field, offshore Taiwan: a case study in migration fractionation. Org. Geochem. 20, 437–462. https://doi.org/10.1016/0146-6380(93)90092-P.

Főzy, I., 2012. Magyarország litosztratigráfiai alapegységei. Jura (Lithostratigraphic Units of Hungary. Jurassic). Hungarian Geological Society, Budapest, pp. 10. (in Hungarian)

George, S.C., Lisk, M., Summons, R.E., Quezada, R.A., 1998. Constraining the oil charge history of the South Pepper oilfield from the analysis of oil-bearing fluid inclusions. Org. Geochem. 29, 631–648. https://doi.org/10.1016/S0146-6380(98)00085-0.

George, S.C., Volk, H., Ahmed, M., 2007. Geochemical analysis techniques and geological applications of oil-bearing fluid inclusions, with some Australian case studies. J. Pet. Sci. Eng. 57, 119–138. https://doi.org/10.1016/j.petrol.2005.10.010.

Goldstein, R.H., Reynolds, T.J., 1994. Systematics of fluid inclusions in diagenetic minerals. Sepm Short Course 31, Society for Sedimentary Geology.

González, M.F., Stull, C.S., López-Linares, F., Pereira-Almao, P., 2007. Comparing asphaltene adsorption with model heavy molecules over macroporous solid surfaces. Energy Fuel 21, 234–241. https://doi.org/10.1021/ef060196+.

Haas, J., Hámor, G., Korpás, L., 1999. Geological setting and tectonic evolution of Hungary. Geol. Hun. Ser. Geol. 24, 179–196.

Haas, J., 2012. Geology of Hungary. Springer Science & Business Media.

Han, Y., Mahlstedt, N., Horsfield, B., 2015. The Barnett Shale: Compositional fractionation associated with intraformational petroleum migration, retention, and expulsion. AAPG Bull. 99, 2173–2202. https://doi.org/10.1306/06231514113.

Han, Y., Horsfield, B., Curry, D.J., 2017. Control of facies, maturation and primary migration on biomarkers in the Barnett Shale sequence in the Marathon 1 Mesquite well, Texas. Mar. Pet. Geol. 85, 106–116. https://doi.org/10.1016/j.marpetgeo.2017.04.018.

Han, Y., Poetz, S., Mahlstedt, N., Karger, C., Horsfield, B., 2018a. Fractionation and origin of N_yO_x and O_x compounds in the Barnett Shale sequence of the Marathon 1 Mesquite well,

Texas. Mar. Pet. Geol. 97, 517–524. https://doi.org/10.1016/j.marpetgeo.2018.07.031.

Han, Y., Poetz, S., Mahlstedt, N., Karger, C., Horsfield, B., 2018b. Fractionation of pyrrolic nitrogen compounds during primary migration of petroleum within the Barnett Shale sequence of Marathon 1 Mesquite Well, Texas. Energy Fuel 32, 4638–4650. https://doi.org/10.1021/acs.energyfuels.7b03488.

Han, Y., Noah, M., Lüders, V., Horsfield, B., Mangelsdorf, K., 2020. NSO-compounds in oil-bearing fluid inclusions revealed by FT-ICR-MS in APPI (+) and ESI (–) modes: A new method development. Org. Geochem. 104113. https://doi.org/10.1016/j.orggeochem.2020.104113.

Han, Y., Horsfield, B., Mahlstedt, N., Noah, M., 2021. Chemostatistic allocation of shale oil production using acidic heterocompounds. AAPG Bull. 105, 2207–2219. https://doi.org/10.1306/06102119035.

Han, Y., Noah, M., Lüders, V., Hartwig, A., Rinna, J., Skeie, J.E., Horsfield, B., Mangelsdorf, K., 2022. Geochemical characteristics of inclusion oils from the Skarv field A segment and their implications for the oil charge and leakage history. Mar. Pet. Geol. 137, 105506. https://doi.org/10.1016/j.marpetgeo.2021.105506.

Heum, O.R., Dalland, A., Meisingset, K.K., 1986. Habitat of hydrocarbons at Haltenbanken (PVT-modelling as a predictive tool in hydrocarbon exploration). In: Spencer, A.M. (Ed.), Habitat of hydrocarbons on the Norwegian continental shelf. Graham & Trotman, pp. 259–274.

Horsfield, B., McLimans, R.K., 1984. Geothermometry and geochemistry of aqueous and oil-bearing fluid inclusions from Fateh Field, Dubai. Org. Geochem. 6, 733–740. https://doi.org/10.1016/0146-6380(84)90094-9.

882 Horsfield, B., Clegg, H., Wilkes, H., Santamaria-Orozco, D., 1998. Effect of maturity on carbazole
883 distributions in petroleum systems: new insights from the Sonda de Campeche, Mexico, and
884 Hils Syncline, Germany. Naturwissenschaften 85, 233–237.
885 https://doi:10.1007/s001140050489.
886 Huba, A.K., Huba, K., Gardinali, P.R., 2016a. Understanding the atmospheric pressure ionization
887 of petroleum components: The effects of size, structure, and presence of heteroatoms. Sci.
888 Total Environ. 568, 1018–1025. https://doi.org/10.1016/j.scitotenv.2016.06.044.
889 Huba, A.K., Gardinali, P.R., 2016b. Characterization of a crude oil weathering series by ultrahigh-
890 resolution mass spectrometry using multiple ionization modes. Sci. Total Environ. 563, 600–
891 610. https://doi.org/10.1016/j.scitotenv.2016.03.233.
892 Hughey, C.A., Rodgers, R.P., Marshall, A.G., Qian, K., Robbins, W.K., 2002. Identification of
893 acidic NSO compounds in crude oils of different geochemical origins by negative ion
894 electrospray Fourier transform ion cyclotron resonance mass spectrometry. Org. Geochem. 33,
895 743–759. https://doi.org/10.1016/S0146-6380(02)00038-4.
896 Hughey, C.A., Galasso, S.A., Zumberge, J.E., 2007. Detailed compositional comparison of acidic
897 NSO compounds in biodegraded reservoir and surface crude oils by negative ion electrospray
898 Fourier transform ion cyclotron resonance mass spectrometry. Fuel 86, 758–768.
899 https://doi.org/10.1016/j.fuel.2006.08.029.
900 Jochum, J., Friedrich, G., Leythaeuser, D., Littke, R., Ropertz, B., 1995. Hydrocarbon-bearing
901 fluid inclusions in calcite-filled horizontal fractures from mature Posidonia Shale (Hils
902 Syncline, NW Germany). Ore Geol. Rev. 9, 363–370. https://doi.org/10.1016/0169-
903 1368(94)00019-K.

Kelemen, S.R., Walters, C.C., Ertas, D., Freund, H., Curry, D.J., 2006. Petroleum expulsion part 3. A model of chemically driven fractionation during expulsion of petroleum from kerogen. Energy Fuel 20, 309–319. https://doi.org/10.1021/ef058023s.

Kim, S., Stanford, L.A., Rodgers, R.P., Marshall, A.G., Walters, C.C., Qian, K., Wenger, L.M., Mankiewicz, P., 2005. Microbial alteration of the acidic and neutral polar NSO compounds revealed by Fourier transform ion cyclotron resonance mass spectrometry. Org. Geochem. 36, 1117–1134. https://doi.org/10.1016/j.orggeochem.2005.03.010.

Larter, S.R., Aplin, A.C., 1995. Reservoir geochemistry: method, application and opportunities. In: Cubitt, J.M., England, W.A. (Eds.), The Geochemistry of Reservoirs. The Geological Society, London, pp. 5–32.

Larter, S.R., Bowler, B.F.J., Li, M., Chen, M., Brincat, D., Bennett, B., Noke, K., Donohoe, P., Simmons, D., Kohnen, M., Allan, J., Telnaes, N., Horstad, I., 1996. Molecular indicators of secondary oil migration distances. Nature 383, 593–597. https://doi.org/10.1038/383593a0.

Leythaeuser, D., Littke, R., Radke, M., Schaefer, R.G., 1988a. Geochemical effects of petroleum migration and expulsion from Toarcian source rocks in the Hils syncline area, NW-Germany. Org. Geochem. 13, 489–502. https://doi.org/10.1016/B978-0-08-037236-5.50056-7.

Leythaeuser, D., Schaefer, R.G., Radke, M., 1988b. Geochemical effects of primary migration of petroleum in Kimmeridge source rocks from Brae field area, North Sea. I: Gross composition of C_{15+}-soluble organic matter and molecular composition of C_{15+}-saturated hydrocarbons. Geochim. Cosmochim. Acta 52, 701–713. https://doi.org/10.1016/0016-7037(88)90331-6.

Leythaeuser, D., Radke, M., Willsch, H., 1988c. Geochemical effects of primary migration of petroleum in Kimmeridge source rocks from Brae field area, North Sea. II: Molecular

926 composition of alkylated naphthalenes, phenanthrenes, benzo-and dibenzothiophenes.
927 Geochim. Cosmochim. Acta 52, 2879–2891. https://doi.org/10.1016/0016-7037(88)90155-X.
928 Li, M., Larter, S.R., Stoddart, D., Bjorøy, M., 1995. Fractionation of pyrrolic nitrogen compounds
929 in petroleum during migration: derivation of migration-related geochemical parameters. In:
930 Cubitt, J.M., England, W.A. (Eds.), The Geochemistry of Reservoirs. The Geological Society,
931 London, pp. 103–124.
932 Liao, Y., Geng, A., 2009. Stable carbon isotopic fractionation of individual *n*-alkanes
933 accompanying primary migration: Evidence from hydrocarbon generation–expulsion
934 simulations of selected terrestrial source rocks. Appl. Geochem. 24, 2123–2132.
935 https://doi.org/10.1016/j.apgeochem.2009.09.002.
936 Liu, W., Liao, Y., Pan, Y., Jiang, B., Zeng, Q., Shi, Q., Hsu, C.S., 2018. Use of ESI FT-ICR MS to
937 investigate molecular transformation in simulated aerobicbiodegradation of a sulfur-rich
938 crude oil. Org. Geochem. 123, 17–26. https://doi.org/10.1016/j.orggeochem.2018.06.003.
939 López-Linares, F., Carbognani, L., González, M.F., Sosa-Stull, C., Figueras, M., Pereira-Almao, P.,
940 2006. Quinolin-65 and violanthrone-79 as model molecules for the kinetics of the adsorption
941 of C_7 athabasca asphaltene on macroporous solid surfaces. Energy Fuel 20, 2748–2750.
942 https://doi.org/10.1021/ef060354x.
943 López-Linares, F., Carbognani, L., Sosa-Stull, C., Pereira-Almao, P., Spencer, R.J., 2009.
944 Adsorption of virgin and visbroken residue asphaltenes over solid surfaces. 1. Kaolin,
945 smectite clay minerals, and athabasca siltstone. Energy Fuel 23, 1901–1908.
946 https://doi.org/10.1021/ef8009102.
947 Lukoczki, G., Schubert, F., Hámor-Vidó, M., 2012. Traces of hydrocarbon migration near

948 Pécsvárad (Mecsek Mts.). Földtani Közlöny 142, 229–241.
949 Mackenzie, A.S., Leythaeuser, D., Schaefer, R.G., Bjorøy, M., 1983. Expulsion of petroleum
950 hydrocarbons from shale source rocks. Nature 301, 506–509.
951 https://doi.org/10.1038/301506a0.
952 Mahlstedt, N., Horsfield, B., Wilkes, H., Poetz, S., 2016. Tracing the impact of fluid retention on
953 bulk petroleum properties using nitrogen-containing compounds. Energy Fuel 30, 6290–6305.
954 https://doi.org/10.1021/acs.energyfuels.6b00994.
955 Mann, U., Hantschel, T., Schaefer, R.G., Krooss, B., Leythaeuser, D., Littke, R., Sachsenhofer,
956 R.F., 1997. Petroleum migration: mechanisms, pathways, efficiencies and numerical
957 simulations. In: Welte, D., Horsfield, B., Baker, D. (Eds.), Petroleum and Basin Evolution.
958 Springer Berlin Heidelberg, pp. 403–520.
959 Marchal, C., Abdessalem, E., Tayakout-Fayolle, M., Uzio, D., 2010. Asphaltene diffusion and
960 adsorption in modified NiMo alumina catalysts followed by ultraviolet (UV) spectroscopy.
961 Energy Fuel 24, 4290–4300. https://doi.org/10.1021/ef1000979.
962 Marshall, A.G., Rodgers, R.P., 2008. Petroleomics: Chemistry of the underworld. Proc. Natl. Acad.
963 Sci. 105, 18090–18095. https://doi.org/10.1073/pnas.0805069105.
964 Mohnhoff, D., Littke, R., Krooss, B.M., Weniger, P., 2016. Flow-through extraction of oil and gas
965 shales under controlled stress using organic solvents: Implications for organic matter-related
966 porosity and permeability changes with thermal maturity. Int. J. Coal Geol. 157, 84–99.
967 https://doi.org/10.1016/j.coal.2015.09.010.
968 Moldowan, J.M., Seifert, W.K., Gallegos, E.J., 1985. Relationship between petroleum composition
969 and depositional environment of petroleum source rocks. AAPG Bull. 69, 1255–1268.

https://doi.org/10.1306/AD462BC8-16F7-11D7-8645000102C1865D.

Murray, A.P., Summons, R.E., Boreham, C.J., Dowling, L.M., 1994. Biomarker and *n*-alkane isotope profiles for Tertiary oils: relationship to source rock depositional setting. Org. Geochem. 22, 521–526. https://doi.org/10.1016/0146-6380(94)90124-4.

Noah, M., Volk, H., Schubert, F., Horsfield, B., 2018. First analysis of polar compounds trapped in fluid inclusions using ultra high resolution mass spectrometry – A proof of concept demonstrated on a case study from the Pannonian Basin (Hungary). Latin American Association of Organic Geochemistry (ALAGO), Salvador, Bahia, Brazil.

Oldenburg, T.B., Wilkes, H., Horsfield, B., Van Duin, A.C., Stoddart, D., Wilhelms, A., 2002. Xanthones—novel aromatic oxygen-containing compounds in crude oils. Org. Geochem. 33, 595–609. https://doi.org/10.1016/S0146-6380(02)00015-3.

Peters, C.A., Hallmann, C., George, S.C., 2018. Phenolic compounds in oil-bearing fluid inclusions: Implications for water-washing and oil migration. Org. Geochem. 118, 36–46. https://doi.org/10.1016/j.orggeochem.2018.02.001.

Peters, K.E., Moldowan, J.M., 1991. Effects of source, thermal maturity, and biodegradation on the distribution and isomerization of homohopanes in petroleum. Org. Geochem. 17, 47–61. https://doi.org/10.1016/0146-6380(91)90039-M.

Peters, K.E., Walters, C.C., Moldowan, J.M., 2005. The Biomarker Guide: Biomarkers and Isotopes in Petroleum Exploration and Earth History, second ed. Cambridge University Press, Cambridge, UK.

Plancher, H., Dorrence, S.M, and Petersen, J.C., 1977. Identification of chemical types in asphalts strongly absorbed at the asphalt-aggregate interface and their relative displacement by water.

992 J. Assoc. Asphalt Paving Technol. 46, 151–175.
993 Poetz, S., Horsfield, B., Wilkes, H., 2014. Maturity-driven generation and transformation of acidic
994 compounds in the organic-rich Posidonia shale as revealed by electrospray ionization Fourier
995 transform ion cyclotron resonance mass spectrometry. Energy Fuel 28, 4877–4888.
996 https://doi.org/10.1021/ef500688s.
997 Poetz, S., Kuske, S., Song, Y., Jweda, J., Michael, E., Horsfield, B., 2020. Using polar nitrogen-,
998 sulphur-and oxygen-compound compositions from ultra-high resolution mass spectrometry
999 for petroleum fluid assessment in the Eagle Ford Formation, Texas. Geol. Soc. Lond., Spec.
1000 Publ. 484, 71–96. https://doi.org/10.1144/SP484-2018-175.
1001 Purcell J.M., Hendrickson C.L., Rodgers R.P., Marshall A.G., 2006. Atmospheric pressure
1002 photoionization Fourier transform ion cyclotron resonance mass spectrometry for complex
1003 mixture analysis. Anal. Chem. 78, 5906–5912. https://doi.org/10.1021/ac060754h.
1004 Radke, M., Welte, D.H., 1983. The Methylphenanthrene Index (MPI): A maturity parameter based
1005 on aromatic hydrocarbons. In: Bjoroy, M. (Ed.), Advances in Org. Geochem. Wiley,
1006 Chichester, pp. 504–512.
1007 Radke, M., Willsch, H., Welte, D.H., 1980. Preparative hydrocarbon group type determination by
1008 automated medium pressure liquid chromatography. Anal. Chem. 52, 406–411.
1009 https://doi.org/10.1021/ac50053a009.
1010 Raucsik, B., Varga, A., 2008. Climato-environmental controls on clay mineralogy of the
1011 Hettangian–Bajocian successions of the Mecsek Mountains, Hungary: an evidence for
1012 extreme continental weathering during the early Toarcian oceanic anoxic event. Palaeogeogr.
1013 Palaeoclimatol. Palaeoecol. 265, 1–13. https://doi.org/10.1016/j.palaeo.2008.02.004.

1014 Raucsik, B., 2012a. Zobákpuszta Sandstone Formation. In: Fozy, I. (Eds.), Jurassic
1015 Lithostratigraphic Units in Hungary, Hungarian Geological Society, Budapest, pp. 149–151.
1016 (in Hungarian)
1017 Raucsik, B., 2012b. Vasas Marl Formation. In: Fozy, I. (Eds.), Jurassic Lithostratigraphic Units in
1018 Hungary, Hungarian Geological Society, Budapest, pp. 152–154. (in Hungarian)
1019 Raucsik, B., 2012c. Hosszúhetény Calcarous Marl Formation. In: Fozy, I. (Eds.), Jurassic
1020 Lithostratigraphic Units in Hungary, Hungarian Geological Society, Budapest, pp. 155–158.
1021 (in Hungarian)
1022 Raucsik, B., 2012d. Rékavölgy Siltstone Formation. In: Fozy, I. (Eds.), Jurassic Lithostratigraphic
1023 Units in Hungary, Hungarian Geological Society, Budapest, pp. 164–167. (in Hungarian)
1024 Raucsik, B., 2012e. Komló Calcareous Marl Formation. In: Fozy, I. (Eds.), Jurassic
1025 Lithostratigraphic Units in Hungary, Hungarian Geological Society, Budapest, pp. 174–176.
1026 (in Hungarian)
1027 Reed, M.G., 1968. Retention of crude oil bases by clay-containing sandstone. Clay Clay Miner. 16,
1028 173–178. https://doi.org/10.1346/CCMN.1968.0160208.
1029 Rullkötter, J., Leythaeuser, D., Horsfield, B., Littke, R., Mann, U., Müller, P.J., Radke, M.,
1030 Schaefer, R.G., Schenk, H.J., Schwochau, K., Witte, E.G., Welte, D.H., 1988. Organic matter
1031 maturation under the influence of a deep intrusive heat source: A natural experiment for
1032 quantitation of hydrocarbon generation and expulsion from a petroleum source rock
1033 (Toarcian shale, northern Germany). Org. Geochem. 13, 847–856.
1034 https://doi.org/10.1016/0146-6380(88)90237-9.
1035 Sandvik, E.I., Young, W.A., Curry, D.J., 1992. Expulsion from hydrocarbon sources: the role of

organic absorption. Org. Geochem. 19, 77–87. https://doi.org/10.1016/0146-6380(92)90028-V.

Schwark, L., Stoddart, D., Keuser, C., Spitthoff, B., Leythaeuser, D., 1997. A novel sequential extraction system for whole core plug extraction in a solvent flow-through cell — application to extraction of residual petroleum from an intact pore-system in secondary migration studies. Org. Geochem. 26, 19–31. https://doi.org/10.1016/S0146-6380(96)00163-5.

Seifert, W.K., Moldowan, J.M., 1980. The effect of thermal stress on source-rock quality as measured by hopane stereochemistry. Phys. Chem. Earth 12, 229–237. https://doi.org/10.1016/0079-1946(79)90107-1.

Seifert, W.K., Moldowan, J.M., 1981. Paleoreconstruction by biological markers. Geochim. Cosmochim. Acta 45, 783–794. https://doi.org/10.1016/0016-7037(81)90108-3.

Sofer, Z., 1984. Stable carbon isotope compositions of crude oils: application to source depositional environments and petroleum alteration. AAPG Bull. 68, 31–49. https://doi.org/10.1306/AD460963-16F7-11D7-8645000102C1865D.

Stanford, L.A., Rodgers, R.P., Marshall, A.G., Czarnecki, J., Wu, X.A., 2007. Compositional characterization of bitumen/water emulsion films by negative-and positive-ion electrospray ionization and field desorption/ionization Fourier transform ion cyclotron resonance mass spectrometry. Energy Fuel 21, 963–972. https://doi.org/10.1021/ef060291i.

Stockhausen, M., Galimberti, R., Di Paolo, L., Elias, R., Gelin, F., Berner, U., Erdmann, M., Pedersen, J.H., Di Primio, R., Schwark, L., 2019. The Expulsinator device: A new approach for a lab-scaled, near-natural generation-and expulsion simulation. J. Pet. Sci. Eng. 177, 69–78. https://doi.org/10.1016/j.petrol.2019.02.031.

Stockhausen, M., Galimberti, R., Elias, R., Di Paolo, L., Schwark, L., 2020. The Expulsinator versus conventional pyrolysis: The differences of oil/gas generation and expulsion simulation under near-natural conditions. Mar. Pet. Geol. 117, 104412. https://doi.org/10.1016/j.marpetgeo.2020.104412.

Stockhausen, M., Galimberti, R., Elias, R., Di Paolo, L., Schwark, L., 2021. Expulsinator assessment of oil/gas generation and expulsion characteristics of different source rocks. Mar. Pet. Geol. 129, 105057. https://doi.org/10.1016/j.marpetgeo.2021.105057.

Taylor, P., Larter, S., Jones, M., Dale, J., Horstad, I., 1997. The effect of oil-water-rock partitioning on the occurrence of alkylphenols in petroleum systems. Geochim. Cosmochim. Acta 61, 1899–1910. https://doi.org/10.1016/S0016-7037(97)00034-3.

Tissot, B.P., Welte, D.H., 1984. Geochemical fossils and their significance in petroleum formation. In: Petroleum Formation and Occurrence, Second ed. Springer, Berlin.

Varga, A., Raucsik, B., Hámor-Vidó, M., Rostási, Á., 2007. Isotope geochemistry and characterization of hydrocarbon potential of black shale from Óbánya Siltstone Formation. Bull. Hung. Geol. Surv. 137. 449–472.

Volk, H., Horsfield, B., Mann, U., Suchy´ , V., 2002. Variability of petroleum inclusions in vein, fossil and vug cements – a geochemical study in the Barrandian Basin (Lower Palaeozoic, Czech Republic). Org. Geochem. 33, 1319–1341. https://doi.org/10.1016/S0146-6380(02)00181-X.

Volk, H., George, S.C., 2019. Using petroleum inclusions to trace petroleum systems – A review. Org. Geochem. 129, 99–123. https://doi.org/10.1016/j.orggeochem.2019.01.012.

Yamamoto, M., Taguchi, K., Sasaki, K., 1991. Basic nitrogen compounds in bitumen and crude

1080 oils. Chem. Geol. 93, 193–206. https://doi.org/10.1016/0009-2541(91)90072-Y.
1081 Yue, H., Vieth-Hillebrand, A., Han, Y., Horsfield, B., Schleicher, A.M., Poetz, S., 2021.
1082 Unravelling the impact of lithofacies on the composition of NSO compounds in residual and
1083 expelled fluids of the Barnett, Niobrara and Posidonia formations. Org. Geochem. 104225.
1084 https://doi.org/10.1016/j.orggeochem.2021.104225.
1085 Ziegs, V., Noah, M., Poetz, S., Horsfield, B., Hartwig, A., Rinna, J., Skeie, J.E., 2018. Unravelling
1086 maturity- and migration-related carbazole and phenol distributions in Central Graben crude
1087 oils. Mar. Pet. Geol. 94, 114–130. https://doi.org/10.1016/j.marpetgeo.2018.03.039.